CO oxidation and oxygen reduction activity of bimetallic Sn-Pt electrocatalysts on carbon: effect of the microstructure and the exclusive formation of the Pt_3Sn alloy

Reaction Kinetics, Mechanisms and Catalysis, Volume 121 (2017) 43-67.

Dorottya Gubán, András Tompos, István Bakos, Zoltán Pászti, Gergely Gajdos, István E. Sajó, Irina Borbáth

ISSN**:** 1878-5190; Source Type: Journal; Original language: English;
Document Type: Article; Publisher: Springer

Akadémiai Kiadó, Budapest, Hungary 2017

The final publication is available at Springer via
http://dx.doi.org/10.1007/s11144-017-1152-8

Corresponding author: Irina Borbáth

Received: 30 November 2016/Accepted: 4 February 2017/Published online: 15 February 2017

Electronic supplementary material:
The online version of this article (doi: 10.1007/s11144-017-1152-8) contains supplementary material, which is available to authorized users.

CO oxidation and oxygen reduction activity of bimetallic Sn-Pt electrocatalysts on carbon: effect of the microstructure and the exclusive formation of the Pt_3Sn alloy

D. Gubán[1], A. Tompos[1], I. Bakos[1], Z. Pászti[1], G. Gajdos[1], I. Sajó[2], I. Borbáth[1*]

[1] *Institute of Materials and Environmental Chemistry, Research Centre for Natural Sciences, Hungarian Academy of Sciences, H-1117 Budapest, Magyar tudósok körútja 2, Hungary*
[2] *University of Pécs, Szentágothai Research Centre, Pécs, H-7624, Ifjúság str. 20, Hungary*

Abstract

Alloy-type Sn-Pt/C electrocatalysts with desired Pt/Sn= 3.0 ratio have been prepared by Controlled Surface Reactions using home-made 20 wt.% Pt/C (20Pt/C) catalysts with different Pt dispersion. Reaction conditions were found for the preparation of highly dispersed 20Pt/C catalysts by modified $NaBH_4$-assisted ethylene-glycol reduction method using ethanol as a solvent. It has been demonstrated that the increase of the heating time in ethanol up to 2 h results in decreasing dispersion of Pt. Upon using highly dispersed 20Pt/C catalyst the exclusive incorporation of Sn onto the Pt sites was achieved resulting in exclusive formation of the Pt-Sn alloy phase. According to *in situ* XPS studies pre-treatment of the air exposed catalyst in H_2 even at 170°C resulted in complete reduction of the ionic tin to Sn^0, suggesting alloy formation. In contrast, the catalyst with lower Pt dispersion cannot be completely reduced even at 350°C, as 10 % of tin still remains in the form of Sn^{4+} surface species. The electrocatalytic performance of both Sn-20Pt/C catalysts in the CO electrooxidation and the oxygen reduction reaction is superior to that of the parent 20Pt/C catalysts. Our data obtained for the oxygen reduction reaction indicate that the small size of the bimetallic nanoparticles in the highly dispersed Sn-20Pt/C catalyst, along with their optimal surface composition, result in increased activity compared to the catalyst with lower dispersion.

Keywords SnPt/C electrocatalysts, Controlled surface reactions, Pt_3Sn, Oxygen reduction reaction, CO electrooxidation

Introduction

Polymer electrolyte membrane fuel cells (PEMFC) offer a very promising solution for environmentally sustainable electric power generation in mobile applications. A major challenge in PEMFC development is the choice of the cathode and anode electrocatalysts, which usually consist of platinum supported on carbon. The Pt/C system is, however, prone to corrosion at high potentials occurring during rapid load change conditions, and sensitive to poisoning by CO, which is a common low level impurity of the hydrogen fuel. As a result, electrocatalysts with acceptable lifetime can only be manufactured with very high Pt loadings. Therefore, a main development goal is to find electrocatalysts with reduced Pt content, enhanced long term stability under operating conditions and affordable price. CO tolerance of the anode electrocatalysts also has to be improved, as CO adsorbs very strongly on Pt, blocking the active sites for the hydrogen oxidation reaction and causing a large decrease in the electrode performance. In order to reduce this poisoning issue, a common approach consists of the utilization of a second oxophilic metal such as Ru, Mo, Ni or Sn [1-5], which are less noble than Pt and thus activate water at lower potential leading to accelerated CO_2

* Corresponding author, Tel.: +36 1 382 6916, email: borbath.irina@ttk.mta.hu, address: H-1519 Budapest, P.O.Box 286, Hungary (Irina Borbáth)

formation rates (the so-called "bifunctional mechanism"). Moreover the activity of bimetallic catalysts may be further modulated by the "electronic (ligand) effect", i.e., the modification of the electronic interaction between Pt and the CO adsorbate. The oxofillic dopant may also hinder dissolution or sintering, which is necessary for maintaining the long term activity of the catalyst.

Pt-Sn bulk alloys are among the most studied binary systems for fuel cell applications [6,7]. However, SnO_2 often exists on the surface of Sn-containing catalysts, which results in the oxidation of the surface of bimetallic nanoparticles. SnO_2 has good corrosion resistance in acidic media and thus is expected to be stable under the working conditions of PEMFCs [8]. In Ref. [9] it has been proposed that during the oxygen reduction reaction (ORR) the SnO_2 nano-islands decorating the Pt_3Sn alloy core nanoparticle surfaces may suppress the over-oxidation of the Pt surface sites and moreover, based on the stability of the SnO_2, would protect the Pt and/or Pt_3Sn core nanoparticles from dissolution.

Exclusive formation of supported Pt-Sn alloy phases with different Pt/Sn ratios can be achieved by using Controlled Surface Reactions (CSRs) between hydrogen adsorbed on Pt sites and tetraethyltin ($Sn(C_2H_5)_4$) [10]. The basic reactions of the CSRs method are the following:

$$PtH_{ads} + Sn(C_2H_5)_4 \rightarrow Pt\text{-}Sn(C_2H_5)_{(4-x)} + x\ C_2H_6 \qquad (1)$$

$$Pt\text{-}\ Sn(C_2H_5)_{(4-x)} + (4-x)/2\ H_2 \rightarrow Pt\text{-}Sn + (4-x)\ C_2H_6 \qquad (2)$$

The use of the above two-step CSR method guarantees the exclusive introduction of tin onto platinum, i.e. the suppression of Sn-support interaction. In case of the Pt-Sn system the net result is the exclusive formation of Sn-Pt alloy phases [11]. Based on CSRs a new method was developed for the preparation of different types of supported E_x-M_y (E= Sn, Ge; M= Pt, Pd, Rh, Ru) catalysts with exclusive formation of metal-metal interaction and high E/M ratios [12-14]. Catalysts prepared in this way showed unique properties in variety of reactions (CO oxidation, naphtha reforming, selective hydrogenation and dehydrogenation of organic compounds [15-19]).

Our results demonstrate [20-22] that upon using CSRs tin anchoring onto the parent 40 wt.% Pt/C resulted in an alloy-type Sn-Pt/C catalysts, which were highly active in both the electrooxidation reactions of CO and C_1-C_2 alcohols. In these studies a clear correlation between the Pt_3Sn alloy phase content and the electrocatalytic performance has been established. It has been shown that the optimal balance between the Pt/Sn ratio, the amount of the fcc Pt_3Sn alloy phase and the metal particle size are responsible for the activity increase in both the CO and alcohol electrooxidation [20-22].

In this work electrocatalysts were prepared by modifying home-made 20 wt.% Pt/C (20Pt/C) parent catalysts of different dispersion. The effect of the Pt dispersion on the structure of the modified catalysts was explored. The activity of the catalysts was compared in both the CO electrooxidation reaction and the ORR.

Experimental

Materials

The organometallic compound (tetraethyltin, $Sn(C_2H_5)_4$), platinum precursor ($H_2PtCl_6 \cdot 6H_2O$) and solvents (*n*-decane and *n*-hexane) were used as received (Sigma-Aldrich). Ethylene-glycol, $NaBH_4$, absolute ethanol, isopropanol, H_2SO_4 and HCl (37 wt.%) were purchased from Molar Chemicals.

Synthesis of home-made 20 wt% Pt/C electrocatalysts

20 wt% Pt/C (20Pt/C) catalysts were prepared by modified $NaBH_4$-assisted ethylene-glycol reduction method using active carbon as a support (CABOT, Black Pearls 2000, 1475

m^2 g^{-1}) and ethanol as a solvent. It should be noted that in Ref. [23] ethylene glycol (EG) was used as a solvent for Pt precursor.

Upon preparation small quantity of the catalysts ("S" type: small batch) 166 mg of the H_2PtCl_6 was solved in absolute ethanol (25 ml) and 200 mg of the support material was suspended in the solution. Upon increasing the temperature up to 65°C the time of the Pt precursor and active carbon stirring in ethanol was varied from short (0.5 h) to prolonged (2 h). Hereupon a solution prepared by the reaction of $NaBH_4$ (590 mg) and EG (7.4 ml) was added dropwise to the suspension at 65°C with stirring. After 3 hours of stirring at 65°C, 15 ml 0.5 M HCl was added to the suspension and stirred for an additional 2.5 hours at RT to deposit the Pt particles onto the support material. The material was washed with water (18.2 MΩ) by centrifugation and dried at 80°C overnight. Upscaling of the preparation of the catalysts ("B" type: big batch) was also attempted, during which the quantities of all components used for the synthesis have been doubled. Preparation details are listed in Table 1.

Synthesis of Sn modified Pt/C catalysts

Three home-made 20 wt.% Pt/C catalysts were modified with $Sn(C_2H_5)_4$ by CSRs in order to obtain electrocatalysts with Pt/Sn= 3.0 ratio. Reaction (1) was performed in a 40 ml stainless steel autoclave at 170°C and P_{H2}= 5 bar using five consecutive tin anchoring periods. The steps of the modification process are described in recent publications [21, 22]; for the convenience of the reader they are also outlined in the Supplementary Material.

After the surface modification the catalysts have been treated in hydrogen atmosphere by Temperature Programmed Reduction (TPR) technique. The final temperature (T_{red}) applied during TPR (reaction (2)) was 250 or 350°C.

Physicochemical characterization

All electrocatalysts were characterized by XRD, TEM, EDS and XPS techniques.

In situ X-Ray Diffraction (XRD) experiments were carried out by a Philips model PW 3710 based PW 1050 Bragg-Brentano parafocusing goniometer in a heatable sample holder as described in the Supplementary Material section. The scans were evaluated with profile fitting methods. The cell parameters of the crystalline phases were determined from the fitted d-values. Crystallite sizes were calculated from reflection line broadening using the Scherrer-equation.

Transmission Electron Microscopy (TEM) studies of the samples were made by use of a FEI Morgagni 268D type transmission electron microscope (accelerating voltage: 100 kV, W-filament). The fresh samples were prepared by grinding and dispersing of the resulted powder in ethanol using an ultrasonic bath. The obtained suspension was dipped onto a carbon coated copper grid. The average diameter was calculated by measuring the diameters of no less than 600-700 randomly selected metal particles from the non-aggregated areas in at least tree micrographs of each sample.

X-ray photoelectron spectroscopy (XPS) measurements were carried out using an EA 125 electron spectrometer manufactured by OMICRON Nanotechnology GmbH (Germany) operated in the Constant Analyser Energy mode with 30 eV pass energy resulting in a spectral resolution of 1 eV. The photoelectrons were excited by MgKα (1253.6 eV) radiation. The samples were first analyzed in the "as received" state. The next measurement was made after reduction in the high pressure cell of the spectrometer in 300 mbar H_2 at different temperatures for 2 hours. Binding energies were referenced to the main component of the C 1s spectrum of the support (graphite at 284.4 eV binding energy). Data were processed using the CasaXPS software package [24] by fitting the spectra with Gaussian-Lorentzian product peaks after removing a Shirley or linear background. Nominal surface compositions were

calculated using the XPS MultiQuant software package [25,26], with the assumption of homogeneous depth distribution for all components. Chemical states were identified by XPS databases [27,28].

Electrochemical characterization

The Sn-Pt/C electrocatalysts were investigated by means of cyclic voltammetry (CV) and adsorbed CO (CO_{ad}) stripping technique in conventional three-electrode electrochemical glass cell using a Biologic SP150 potentiostat and the EC-LAB software package. The working electrode was prepared by supporting the electrocatalysts on a glassy carbon (GC) electrode (d = 0.3 cm, geometric surface area A = 0.0707 cm^2). Before each test the glassy carbon disc was polished with 0.05 μm alumina to obtain a mirror finish, followed by ultrasonic cleaning in water (18.2 MΩ cm), isopropanol and again water to remove any traces of organic impurities.

The samples under study were deposited onto the glassy carbon by means of a catalyst ink. 2 mg of the electrocatalyst, 0.4 ml of isopropanol, 1.592 ml of water (18.2 MΩ cm) and 8 μl of Nafion solution (DuPont™ Nafion® PFSA Polymer Dispersions DE 520) were dispersed in an ultrasonic bath for 45 minutes, resulting in a homogeneous ink. After ultrasonic dispersion an 3.6 μl aliquot has been dropped over the glassy carbon surface and dried in air leading to a homogeneous coating. Pt was used as counter electrode. The reference electrode was reversible hydrogen electrode (RHE). The applied electrolyte was 0.5 M H_2SO_4. Prior to the measurements, the electrode was activated by potential cycling 10 times in the range 50 and 1000 mV (vs. RHE) at a scan rate of 100 mV s^{-1}. After the activation procedure, cyclic voltammetric measurements were done in the potential range of 50-1000 mV (vs. RHE) at a scan rate of 10 mV s^{-1}.

The amount of CO_{ad} over the catalysts has been measured by CO stripping voltammetry in 0.5 M H_2SO_4. Gaseous CO was fed into the cell for 30 min while maintaining the electrode potential constant at 50 mV. After CO removal from the solution (Ar purge for 30 min), the working electrode was subjected to a cyclic voltammetric measurement at a 10 mV s^{-1} scan rate between 50 and 1000 mV. The amount of adsorbed CO was evaluated by integration of the CO stripping peak.

The electrochemically active Pt surface area (ECSA) values were calculated from the charge associated with a CO monolayer adsorbed onto the Pt nanoparticles ($ECSA_{CO}$, using the assumption that oxidation of a full monolayer of linearly adsorbed CO requires 420 μC cm^{-2}) and from the hydrogen adsorption/desorption region ($ECSA_H$) observed on the CVs. For $ECSA_H$ calculations a charge of 210 μC cm^{-2} is widely accepted and used [29].

Catalytic activity of the catalyst samples was tested in oxygen reduction reaction (ORR) by rotating disk electrode (RDE) technique in O_2 saturated 0.5 M H_2SO_4 solution at ambient temperature and pressure. GC electrode of 5 mm diameter (geometric surface area: 0.196 cm^2) was used in these measurements. 10 μl catalyst ink was dropped on the freshly polished GC electrode which resulted in about 10 μg cm^{-2} Pt loading. Polarization curves were recorded by sweeping the potential between 300 and 1000 mV with 10 mV s^{-1} sweep rate, rotating the electrode at 225, 400, 625, 900 and 1225 rpm. Data were obtained from the negative scans. In order to characterize the surface state of the catalysts, before and after the RDE measurements 10 CVs between 50 and 1000 mV potential limits in Ar saturated electrolyte were also measured.

Relative errors were calculated as the standard deviation of at least three independent measurements. The protocol of the electrochemical measurements was previously tested on commercially available standard 20 wt% Pt/C electrocatalyst (Quintech, C-20-Pt) with respect to the specifications from the manufacturer.

Results and discussion

Preparation of 20 wt% Pt/C electrocatalysts

Upon the preparation of home-made Pt/C catalysts the aim was (i) to adapt the method for using ethanol as a solvent and (ii) to scale-up the amount of the catalyst prepared in one portion. It should be noted that increase of the reduction temperature from room temperature to 65°C permits to decrease the overall reaction time. One of the relevant experimental variables is the duration of this reduction. TEM images of the home-made 20 wt.% Pt/C catalysts reduced for 2 h and 0.5 h are depicted in Fig. 1 along with histograms displaying the particle size distribution. Preparation conditions and properties of the home-made 20 wt.% Pt/C catalysts are presented in Table 1.

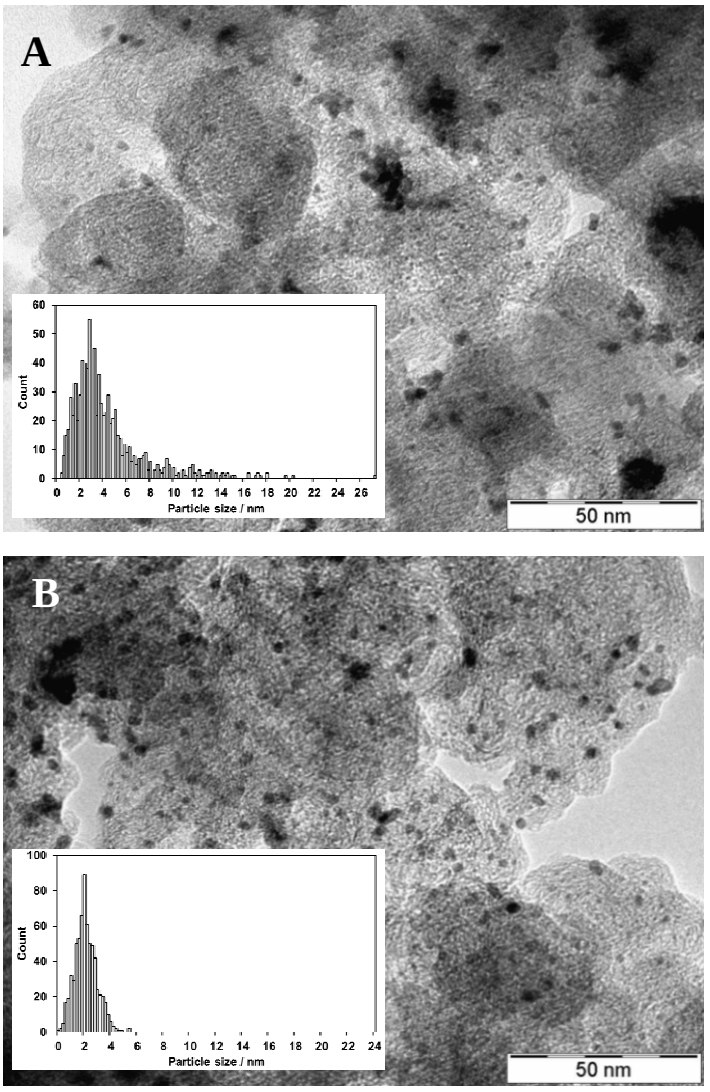

Fig. 1 TEM images and histograms of particle size distribution for (A) 20Pt/C (B-2); and (B) 20Pt/C (S-0.5) catalysts.

The results show that the duration of heating to 65°C before the addition of the $NaBH_4$ and EG mixture has crucial effect on the morphology of the metal deposits. As emerges from Table 1 prolonged stirring of Pt precursor and active carbon in ethanol at 65°C before addition of the mixture of EG with $NaBH_4$ has negative influence on the dispersion of the Pt nanoparticles.

Table 1. Preparation conditions and properties of the home-made 20Pt/C catalysts.

Catalyst [a]	W_C, [b] mg	W_{Pt}, [c] mg	Time, [d] h	TEM, nm	$E_{CO,onset}$, mV	$E_{CO,max}$, [e] mV	$ECSA_{CO}$, m^2/g_{Pt}
20Pt/C (S-2)	200	166	2	5.3±3.3	625	765	46.8 ± 1.1
20Pt/C (B-2)	400	333	2	4.4±3.2	625	775	45.3 ± 2.6
20Pt/C (S-0.5)	200	166	0.5	2.0±1.1	615	785	77.0 ± 7.7

[a] Denomination of the different samples in parenthesis indicates important parameters of the synthesis. Accordingly, the first letters "S" or "B" reflect to the amount of catalyst desired to be prepared (S: small batch, B: big batch), whereas the number shows the time of heating the ethanol solution containing the Pt precursor and carbon support before addition of the $NaBH_4$ and EG mixture (in hours);
[b] Amount of the active carbon support;
[c] Amount of the Pt precursor;
[d] The time of heating ethanol solution containing Pt precursor and carbon support before $NaBH_4$ and EG mixture addition;
[e] The position of the main CO_{ad} stripping peak.

It is known that EG as a solvent, reducing agent and stabilizer has received great attention. In obtaining metal particles with narrow size distribution, its stabilizer function is especially important. Glycolate produced from the EG by oxidation interacts with the metal nanoparticles and inhibits their coalescence; as a result, well-dispersed Pt-based electrocatalysts, with narrow particle-size distribution are obtained without any additional stabilizers [30].

Upon using of modified $NaBH_4$-assisted EG reduction method Pt is reduced using the complex produced by mixing EG with $NaBH_4$ ($Na^+B^-(OCH_2CH_2OH)_4$ [31,32]). It has been reported [31,32] that the reducing strength of this complex is stronger than that of ethylene glycol, and as a result, the Pt precursor can be completely reduced even at room temperature. Furthermore, this complex, as a stabilizer, has bulky characteristics and a strong affinity for Pt nanoparticles. The fast reduction along with the stabilizing effect ensures the formation of very small Pt nanoparticles with a narrow particle-size distribution.

According to the literature [33-37] at elevated temperature ethanol itself is able to reduce Pt-group metals. Thus, during a long annealing period in ethanol, Pt has enough time to nucleate in the absence of the stabilizing agent, resulting in uncontrolled particle growth. Even the possibility of homogeneous nucleation cannot be ruled out; the raspberry-like features may be the results of a liquid phase nucleation process accompanied by incomplete coalescence, probably encouraged by the subsequent fast reduction upon addition of the EG and $NaBH_4$. This was a reason that upon the preparation of the 20Pt/C (S-0.5) catalyst the time of heating ethanol solution containing Pt precursor and carbon support before $NaBH_4$ and EG mixture addition was minimized to 0.5 h. As emerges from Table 1 this catalyst has the smallest size of the Pt nanoparticles. The uniform distribution of spherical Pt particles with mean diameter of (2.0 ± 1.1) nm was verified via TEM imaging (Fig. 1B).

According to the TEM results, the morphology of the 20Pt/C (S-2) (image not shown) and the 20Pt/C (B-2) (Fig. 1 A) catalysts is essentially identical, thus upscaling does not alters the properties of the Pt particles. As emerges from Table 1, in both cases prolonged stirring (2 hours) of Pt precursor and carbon support in ethanol solution at 65°C results in an increase of the size of the Pt nanoparticles. TEM image (see Fig. 1A) reveals that some of the small Pt particles are separated while a significant portion of them are included in raspberry-like agglomerates.

The electrochemical behavior of the Pt/C electrocatalysts prior to modification by Sn was determined in cyclic voltammetry and CO_{ad} stripping (see Fig. S1 in the Supplementary Material, section 3). As can be seen from Table 1 the onset potential ($E_{CO,onset}$) for the oxidation of CO on the home-made Pt/C catalysts was about 615-625 mV with the main CO_{ad} stripping peak maximum ($E_{CO,max}$) at about 765-785 mV.

According to literature data CO stripping voltammetry provides a fingerprint of the particle size distribution and the extent of particle agglomeration in carbon-supported Pt catalysts [38]. The presence of two electrooxidation peaks at 760 and 840 mV in Pt-based catalysts was ascribed by Maillard *et al.* [39] to the CO oxidation on Pt nanoparticles with different size and structures (the peaks at 840 mV and 760 mV were related to small isolated single crystalline Pt nanoparticles and Pt agglomerates, respectively [38]). Enhanced catalytic activity of Pt agglomerates composed of interconnected nm-sized metal grains was ascribed to high concentration of surface defects in Ref. [38]. Similar tendency was observed in the present study. Electrochemical CO monolayer oxidation is influenced by the size of Pt nanoparticles, the smaller the particle size, the higher the reaction overpotential (see Table 1), while the shape of the CO oxidation peak (Fig. S1 B in the Supplementary Material) reflects the morphological differences between the catalysts.

As presented in Table 1, the best electrochemical performance in CO_{ad} stripping was observed on the 20Pt/C (S-0.5) catalyst. As can be seen from Fig. S1 and Table 1 the behavior of the 20Pt/C (S-2) and the 20Pt/C (B-2) electrocatalysts was quite similar. Based on both TEM and electrochemical characterization results it can be concluded that preparation of the double amount of the 20Pt/C catalyst was successfully done.

Modification of home-made 20 wt.% Pt/C catalysts with tetraethyltin

In our earlier study it has been demonstrated [21] that upon the modification of the high-load Pt catalysts with tin the application of the consecutive anchoring reactions using lower initial tetraethyltin concentration was recommended.

Table 2. Influence of the final temperature of the H_2 treatment (T_{red}) of the Sn-20Pt/C catalysts on the particle size and electrochemical performance (for comparison results obtained on the parent home-made 20Pt/C catalysts are also included).

Catalyst	T_{red}, °C	TEM, nm	$E_{CO,onset}$, mV	$ECSA_{CO}$, [b] m^2/g_{Pt}
20Pt/C (S-2)	-	5.3±3.3	625	46.8 ± 1.1
Sn-20Pt/C (S-2)	without TPR [a]	7.1±3.7	205	15.0 ± 0.3
20Pt/C (B-2)	-	4.4±3.2	625	45.3 ± 2.6
Sn-20Pt/C (B-2)	without TPR [a]	7.5±3.1	205	21.7 ± 2.6
Sn-20Pt/C (B-2)	250	6.6±3.7	195	32.1 ± 3.1
20Pt/C (S-0.5)	-	2.0±1.1	615	77.0 ± 7.7
Sn-20Pt/C (S-0.5)	without TPR [a]	n.m.	205	63.3 ± 1.2
Sn-20Pt/C (S-0.5)	250	2.4±1.1	205	56.7 ± 1.2
Sn-20Pt/C (S-0.5)	350	3.4±1.4	210	62.6 ± 0.8

Amount of the 20Pt/C catalyst: 0.2 g; solvent: *n*-decane (V_{C10H22}= 10 ml); concentration of $SnEt_4$ solution: $[SnEt_4]_0$= 0.031 M; total amount of tin introduced during tin anchoring step I: $SnEt_4$= 0.07 mmol.

[a] Without TPR: catalyst used after modification and drying procedure, without high-temperature treatment in H_2;

[b] $ECSA_{CO}$ values were calculated from the CO-stripping measurements;

n.m., the sample was not measured.

Moreover the use of extremely high SnR_4 concentration should be avoided, since it can lead to the concentration gradient of the anchored modifier [40]. The use of consecutive reaction steps avoids any inhomogeneity of the modifier over the metallic particles. Experimental results related to tin anchoring onto the parent 20Pt/C catalysts are summarized in Table 2. Considering increased number of the surface functional groups of the Black Pearls 2000 carbon support five tin anchoring steps were used.

Microstructure of the Sn-20Pt/C electrocatalysts

TEM images and histograms of particle size distribution for the Sn-modified systems based on the two types of home-made parent catalysts are presented in Fig. 2.

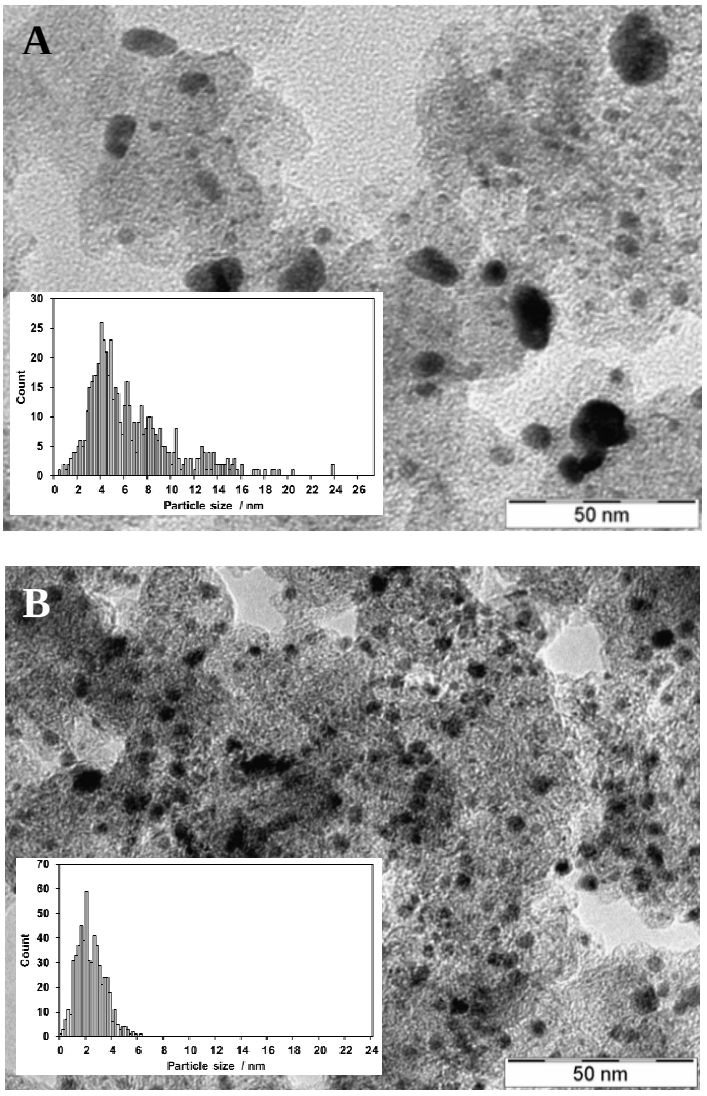

Fig. 2 TEM images and histograms of particle size distribution for (A) Sn-20Pt/C (B-2) sample studied after tin anchoring step I without any high-temperature treatment; and (B) Sn-20Pt/C (S-0.5) catalysts reduced at T_{red}= 250 °C.

As shown in Fig. 2 and Table 2 the modification of home-made 20Pt/C monometallic catalysts with tin results in some increase of the size of bimetallic particles and the increase is more pronounced on the catalysts with lower Pt dispersion (images for 20Pt/C (S-2) and

20Pt/C (B-2) are essentially identical). As shown in Fig. 2A upon tin introduction the raspberry-like Pt agglomerates, observed in Figs. 1A coalesce into large islands.

It is necessary to mention that catalysts supported on functionalized carbon could not tolerate high-temperature thermal treatment, due to the instability of surface oxygen groups of the support [41,42]. It has been reported [43] that the strong (e.g. carboxylic, anhydride groups) and weak acid groups (e.g. lactone, phenol, carbonyl groups) decomposed at 273^{o}C and 407^{o}C, respectively. Even if these surface groups help in ensuring high dispersion of Pt during low temperature preparation, their sensitivity to the annealing temperature negatively influences the final dispersion of metallic Pt and its resistance to sintering if the preparation of the catalyst requires annealing at elevated temperatures. In this respect the dispersion of metallic platinum and resistance to sintering are strongly affected by the T_{red} applied in step II. Even upon reduction at 250°C some part of the stronger acid groups can be decomposed. Thus catalysts with enhanced resistance against sintering can be obtained if the density of the temperature sensitive functional groups is limited, thus upon preparation of the home-made 20Pt/C parent catalysts we used "as received" Black Pearls 2000 carbon (without any additional functionalization treatment).

The influence of the high-temperature treatment in hydrogen on the nanoparticles size was demonstrated on the Sn-20Pt/C (B-2) catalyst (see Table 2). The Sn-20Pt/C (B-2) catalyst was studied after tin anchoring step I (without TPR) and after reduction at 250 °C for 2 h. As shown in Table 2 the reduction of catalyst at T_{red}= 250°C results in the minor decrease of the bimetallic nanoparticles size. In our previous study [21] reversible interconversion of PtSn ↔ Sn^{4+} + Pt in the presence of O_2 and H_2 was convincingly demonstrated by *in situ* XPS studies. In air stored samples some part of tin (in SnO_x form) is located on the platinum-support interface, but after high-temperature reduction all tin (as Sn^0) are alloyed with Pt, thus the decrease of the size of bimetallic nanoparticles is reasonable.

We demonstrated earlier [21] that the increase of the T_{red} from 250 up to 350°C results in an increase of the average crystallite size of the bimetallic nanoparticles. Based on these observations the influence of two final temperature of the H_2 treatment (T_{red}= 250 and 350°C) on the size of the nanoparticles of the Sn-20Pt/C (S-0.5) sample was also studied (see Table 2). As shown in Table 2 upon increasing temperature from 250°C up to 350°C during treatment of the Sn-20Pt/C (S-0.5) catalyst, some minor increase of the bimetallic particles size was also observed, but this increase was not as pronounced as previously observed for the Sn-modified commercial 40 wt% Pt/C (Quintech) in Ref. [21].

SEM and EDS analysis (Fig. S2 in the Supplementary Material) of different regions of the Sn-20Pt/C (S-2) catalyst sample reveals the coexistence of Sn and Pt particles with Pt content of 22.6 ± 1.4 wt.% and Sn content of 3.8 ± 0.6 wt.% of Sn which agrees closely with expected values (Pt= 20 wt.% and Sn= 4 wt.%). The Pt/Sn atomic ratio is 3, which agrees well with the nominal Pt/Sn atomic ratio. No evidence of Sn segregation was seen.

XRD studies of the Sn-20Pt/C (S-0.5) electrocatalyst

It is well known that upon increasing tin content the lattice parameter changes linearly from 3.9231 Å for pure Pt (PDF#04-0802) to 4.0015 Å for Pt_3Sn alloy (PDF#35-1360). Thus the incorporation of tin into the fcc structure of platinum results in shift of the peaks to lower 2θ values [20]. The Sn-modified 20Pt/C (S-0.5) catalyst was studied after treatment in H_2 at T_{red}= 350°C by *ex situ* and *in situ* XRD techniques (see Table 3 and Supplementary Material, section 5). Considering the small particle size and narrow particle size distribution, and noting that we were unable to detect the superlattice reflections for this sample, we have decided to use a single-phase model in the evaluation of the XRD data, instead of assuming the coexistence of a Pt-rich fcc solid solution and Pt_3Sn [21].

Table 3. Lattice parameter and particle size calculated for the Sn-20Pt/C (S-0.5) catalyst reduced before *(ex situ)* and during *(in situ)* XRD measurement (details see experimental part).

Samples	Reduction	Lattice parameter, Å	Average crystallite size [b], nm
1	*ex situ* [a]	a: 3.936	7.3
2	*in situ*	a: 3.955	6.6

[a] Before XRD measurement the sample was reduced at 350°C for 2 h using TPR technique and stored in air;
[b] The Pt particle size of the parent 20Pt/C (S-0.5) catalyst: 2.0±1.1 nm (determined by TEM).

As shown in Table 3 the lattice parameter value (a= 3.936 Å) obtained after the *ex situ* reduction at 350°C was quite close to lattice parameter of the saturated $Pt_{90}Sn_{10}$ solid solution phase (3.934 Å) [44]. *In situ* XRD experiments reveal the gradual shift of the (Sn)-Pt (111) reflection towards lower angles as the reduction temperature is increased, indicating the dissolution of Sn into the bulk of the Pt particles at elevated reduction temperatures (Fig. S3 in the Supplementary Material). Reflections assignable to Sn oxides were not found. However, since it is well established that under oxidizing conditions Sn tends to segregate to the surface of the alloy particles where it transforms into an oxide form [45,46] and considering that the single phase model suggests the presence of a Pt-rich solid solution phase with much less Sn content than the Pt/Sn= 3 ratio established by EDS, the presence of highly dispersed SnO_x in an "X-ray amorphous" form is expected.

Slight difference observed in the average crystallite size after the *ex situ* and *in situ* treatments are in good agreement with our *in situ* XPS results demonstrating the reversible interconversion of the ionic SnO_x forms located on the platinum-support interface into the Pt-Sn alloy phase in the presence of H_2, thus decreasing the size of bimetallic nanoparticles.

XPS analysis of the Sn-20Pt/C electrocatalysts

XPS was used to assess the surface composition of the Sn-20Pt/C electrocatalysts investigated in this study. After modification of the parent catalysts in hydrogen atmosphere, all tin is in Sn^0 state, existing probably in the form of ad-atoms and /or in a form of Sn-Pt alloy phases [21]. However, contact of the samples with air during washing, drying and storage results in oxidation of some part of tin (or even platinum) in Sn-Pt/C catalysts [21]. Accordingly, to get information about the reduction behavior of the catalysts, *in situ* reduction experiments were also carried out in the high pressure chamber of the electron spectrometer, during which air exposure was excluded.

Table 4 contains the compositional and chemical state data for the samples in the as received state and after reductive treatments in 300 mbar H_2 for 2 h at the indicated temperatures.

In identifying the chemical states of tin, in addition to the binding energy of the Sn $3d_{5/2}$ peak, the kinetic energy of the Sn $M_4N_{45}N_{45}$ Auger transition was also considered (see Fig. 3).

Accordingly, the Sn $3d_{5/2}$ peak of SnO_2 arises at a binding energy of 487.1 eV and the well-defined, narrow $M_4N_{45}N_{45}$ Auger peak is at 431.6 eV; their sum, the so called modified Auger parameter, which is a sensitive probe for the ionic state of Sn, is at 918.7 eV. In bulk metallic tin the $3d_{5/2}$ binding energy shifts to 485.0 eV and the $M_4N_{45}N_{45}$ transition appears at a kinetic energy of 437.4 eV, giving an Auger parameter value of 922.4 eV.

Table 4. Summary of the XPS analysis of the Sn-20Pt/C (S-0.5) and the Sn-20Pt/C (S-2) samples (the samples were investigated after reduction at 350°C for 2 h and air storage).

Treatment	Element (photoelectron peak, binding energy (eV), chemical state, concentration (atomic %))											
	Pt $4f_{7/2}$			Sn $3d_{5/2}$			O 1s			C 1s		
	BE	Ch. state	Cc.	BE	Ch. state	Cc.	BE	Ch. state	Cc.	BE	Ch. state	Cc.
Sn-20Pt/C (S-0.5)												
as received	71.2 72.4	Pt^0 90% Pt^{2+} 10%	1.0	486.7 485.5	$Sn^{4+,2+}$ 88% Sn^0 12%	0.5	530.8 532.3	M-ox -OH, $-CO_x$ water	4.3	284.4	Gra-phite	94.2
Reduction, RT, 2 h	71.0	Pt^0 100%	1.1	487.2 485.3	Sn^{4+} 40% Sn^0 60%	0.5	530.9 532.5	M-ox -OH, $-CO_x$	3.7	284.4	Gra-phite	94.8
Reduction, 170°C, 2 h	71.3	Pt^0 100%	1.1	485.4	Sn^0 100%	0.3	532.7	-OH, $-CO_x$	2.7	284.4	Gra-phite	95.9
Reduction, 350°C, 2 h	71.2	Pt^0 100%	1.1	485.4	Sn^0 100%	0.4	533.2	-OH, $-CO_x$	0.9	284.4	Gra-phite	97.6
Sn-20Pt/C (S-2)												
as received	71.3 72.5	Pt^0 88% Pt^{2+} 12%	0.8	486.7	$Sn^{4+,2+}$ 100%	0.4	531.1 533.1	M-ox -OH, $-CO_x$ water	3.5	284.4	Gra-phite	95.3
Reduction, 200°C, 2 h	71.3	Pt^0 100%	0.8	487.0 485.4	Sn^{4+} 12% Sn^0 88%	0.3	531.0 533.1	M-ox -OH, $-CO_x$	4.0	284.4	Gra-phite	94.9
Reduction, 250°C, 2 h	71.3	Pt^0 100%	0.8	486.9 485.3	Sn^{4+} 7% Sn^0 93%	0.3	530.9 533.1	M-ox -OH, $-CO_x$	3.0	284.4	Gra-phite	95.9
Reduction, 350°C, 2 h	71.2	Pt^0 100%	0.9	486.9 485.3	Sn^{4+} 10% Sn^0 90%	0.4	530.9 533.1	M-ox -OH, $-CO_x$	1.7	284.4	Gra-phite	97.0

M-ox stands for metal oxide
Cc. stands for Concentration (atomic %)

Sample Sn-20Pt/C (S-0.5) even in the *as received* state contains some Sn^0 (around 12 %, see Fig. 3). The majority of tin is oxidized, giving a $3d_{5/2}$ peak at 486.7 eV binding energy. At the same time the $M_4N_{45}N_{45}$ Auger peak appearing around 432.1 eV is rather broad and featureless, suggesting the presence of more than one chemical state for tin. It is possible that tin deposited exclusively onto Pt during the CSRs becomes only incompletely oxidized upon

air exposure, resulting in a mixture of Sn^{2+} and Sn^{4+} species, as literature tends to assign Sn $3d_{5/2}$ signals around 486.0-486.5 eV to Sn^{2+}-like species, rather than to Sn^{4+} [47,48]. On the other hand, charge transfer from Pt to the intimately coupled SnO_x cannot be ruled out. Nevertheless, the observed shift of the Sn $3d_{5/2}$ peak to lower binding energy is characteristic for the oxidized Sn-Pt alloy particles [49]. Pt is mostly metallic with a small amount of Pt^{2+} ions. In weight percent this sample contains 14 wt.% of Pt and 4 wt.% of Sn. The Pt/Sn atomic ratio is around 2.2 (see Table 4).

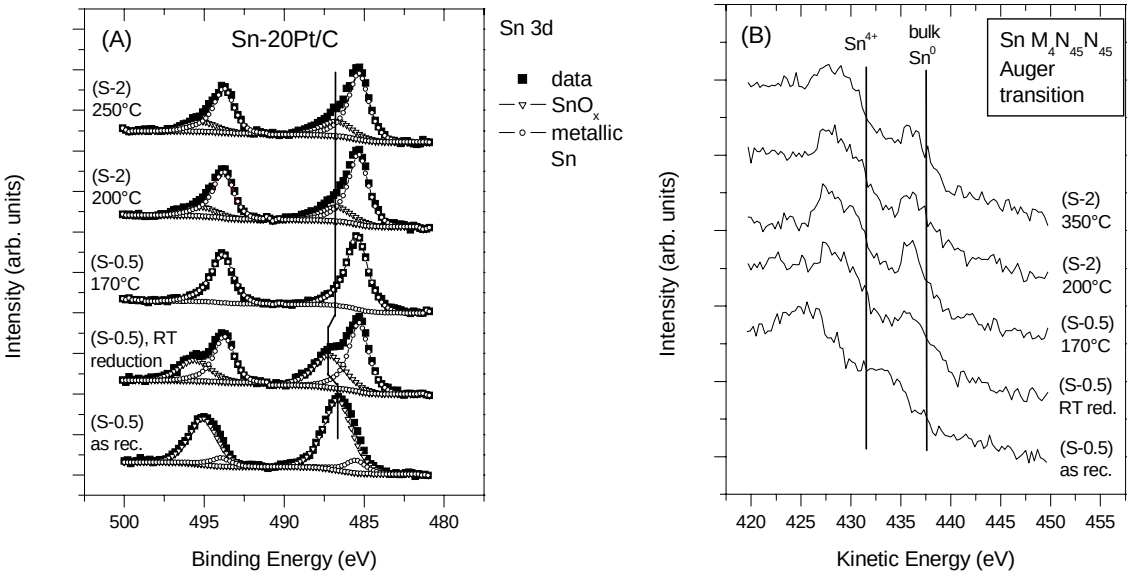

Fig. 3 (A): Selected Sn 3d core level and (B): Sn MNN Auger spectra of the Sn-20Pt/C-(S-0.5) and the Sn-20Pt/C-(S-2) samples at different stages of the *in situ* reduction experiments. Sample identifiers and temperature of reduction in 300 mbar H_2 for 2 hours are indicated. The Sn 3d spectra are corrected for the $MgK\alpha_{3,4}$ satellites.

The *as received* state of sample Sn-20Pt/C (S-2) is very similar. The only differences are that no metallic Sn contribution can be detected and the apparent metal content calculated from the photoelectron peak intensities is notably smaller. In weight percent this sample contains 11 wt.% of Pt and 3 wt.% of Sn; the Pt/Sn ratio is exactly 2.

In the case of sample Sn-20Pt/C (S-0.5) the first *in situ* reduction step was carried out at room temperature (RT). After exposure to 300 mbar H_2 at RT for 2 h the Pt become fully metallic and about 60 % of the tin content was reduced to Sn^0 showing a Sn $3d_{5/2}$ binding energy of 485.3 eV. This value is somewhat high for bulk metallic Sn (485.0 eV or below), but corresponds well to those reported for Pt-Sn alloys [48-50]. The somewhat low Sn $M_4N_{45}N_{45}$ Auger kinetic energy (436.0 eV giving an Auger parameter of 921.5 eV) is still compatible with a metallic environment; the shift from the bulk metallic value is again indication of Sn-Pt alloy formation. The Pt/Sn atomic ratio slightly increased to around 2.5. The smaller than expected Pt/Sn ratio indicates that metallic tin still remains a surface species. According to the literature, surface segregation of tin in Pt-Sn alloys is a known property [50,51]; the nature of the segregation seems to be also related to the Pt particle size [52]. As it is shown in Fig. 3, the contribution from oxidized tin after RT reduction shifts to a binding energy characteristic for SnO_2, suggesting that the intimate coupling between tin oxide and Pt became destroyed during reduction.

The next reduction step of the sample Sn-20Pt/C (S-0.5) was carried out at 170°C, after which the tin content is fully metallic, suggesting alloy formation and the intended Pt/Sn ratio of 3.0 can be measured.

Apart from a decrease of the oxygen content, no significant change was observed upon reduction at 350°C.

The Sn-20Pt/C (S-2) sample was first reduced at 200°C. As it turns out both from the Table 4 and Fig. 3, this treatment does not result in complete reduction of the tin content, in contrast to what was seen for the Sn-20Pt/C (S-0.5) sample. While the major Sn $3d_{5/2}$ contribution appears at 485.4 eV binding energy (characteristic for alloyed tin), a minor peak at 487.0 eV shows the presence of Sn^{4+} species (see Fig. 3). As the result of the simultaneous presence of highly oxidized and reduced Sn species, the Sn $M_4N_{45}N_{45}$ Auger line becomes particularly broad and featureless (see Fig. 3). The incomplete reduction of tin is also reflected by the presence of a metal-oxide related O 1s contribution. At the same time Pt becomes fully metallic. The Pt/Sn (atomic) ratio is around 2.3, i.e. the apparent Sn content decreased a little, indicating the less segregated nature of Sn in the reduced system.

Reduction at 250°C in 300 mbar H_2 for 2 h results in only a minor decrease of the oxidized tin contribution, accompanied by a slight increase of the Pt/Sn ratio to 2.4. Even reduction at 350°C is not enough for removing the oxidized forms of tin, as essentially unchanged composition and chemical state data were obtained.

Considering the electron microscope results, the surprisingly low metal content measured by XPS for the Sn-20Pt/C (S-2) sample is the result of the low dispersion of Pt. If the metal content is present in features significantly larger than roughly 10 nm, atoms in the inside of those particles become inaccessible for XPS. The resulting apparent metal concentration will therefore be lower than the actual value determined by less surface specific techniques.

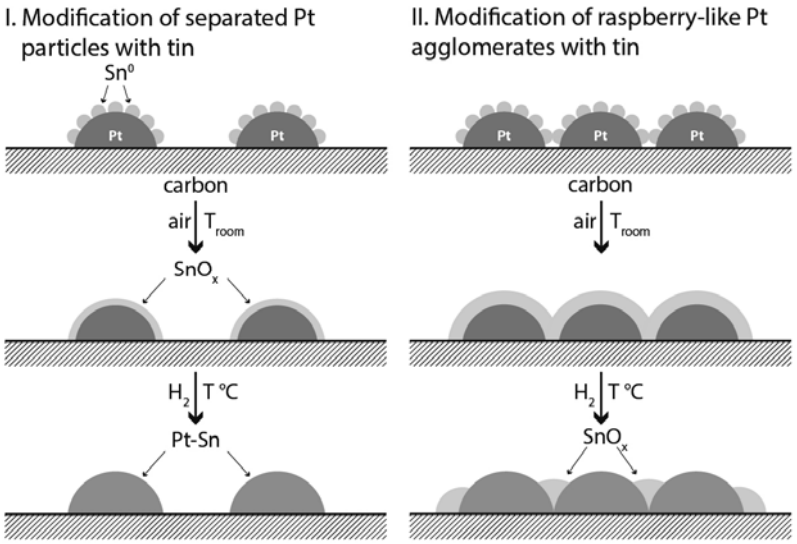

Scheme 1. Proposed model of the presence of various forms of tin in Sn-20Pt/C catalysts with different platinum dispersion: (a) after tin anchoring reaction at 170°C using P_{H2}= 5 bar; (b) after air exposition at room temperature for 2 hours; (c) after *in situ* H_2 treatment of air stored samples at $T_{red} \geq 170$°C. Modification of the home-made 20Pt/C catalysts containing highly dispersed separated Pt particles (left) and raspberry-like Pt agglomerates (right) with $SnEt_4$ by CSRs. Experimental evidences have been found supporting both (**I**) and (**II**) reaction pathways.

At the same time, the non-reducible tin species can probably be imagined as SnO_2 particles in the immediate vicinity of the Pt-Sn alloy particles, which, however, are less strongly coupled to the Pt-containing features. The presence of Sn atoms with only Sn neighbors (Sn islands) in the Sn-20Pt/C catalysts can be a reason of the existence of tin in a form of unreducible SnO_2 phase even after reduction at 350°C. Our results on Sn-20Pt/C (S-0.5) or Sn-modified commercial 20Pt/C (Quintech) catalysts [21] demonstrate that all tin atoms which are in the close vicinity to Pt can be easily reduced to metallic state. Consequently, in the Sn-20Pt/C (S-2) catalyst the presence of different types of surface Sn atoms can be expected: Sn with Pt neighbors and Sn with only Sn neighbors (Sn islands). The low dispersion of Pt and the presence of the Pt raspberry-like agglomerates in the parent catalyst can be a reason for some part of tin appearing on the platinum-support interface; these Sn species may fill the space between the Pt particles included in agglomerates.

Based on the XPS results obtained on two types of Sn-modified catalysts with different dispersion the schematic view of the transformation of various forms of tin after different treatments was shown in Scheme 1.

Electrochemical performance of the Sn-20Pt/C electrocatalysts

In Fig. 4 cyclic (left panels) and CO_{ads} stripping (right panels) voltammograms obtained on the three home-made parent 20Pt/C catalysts with different Pt dispersion (S-2, B-2 and S-0.5) and the corresponding Sn-modified counterparts are presented.

All Pt/C electrocatalysts (short dashed lines) have characteristic hydrogen adsorption/desorption features in the range between $0.05 < E < 0.4$ V and enlarged double layer region, which is related to the big surface area and the increased number of the surface functional groups of the carbon support. As shown in Fig. 4 the double-layer region signal obtained on all tin-modified samples was almost identical to that of parent 20Pt/C catalysts.

The CVs of the tin-modified samples without (solid lines) or after (dotted or dashed lines) TPR showed a rather suppressed hydrogen adsorption/desorption region. A site-blocking effect caused by tin segregation is a reason of the pronounced decrease of H_2 adsorption/desorption, as XPS revealed a segregated tin-oxide layer on all Sn-Pt samples after air exposure. As can be seen from Fig. S4A of the Supplementary Material this site-blocking effect is more pronounced in the case of catalysts containing raspberry-like Pt agglomerates ((S-2) and (B-2)), where XPS data indicate the presence of surface SnO_2 even after reduction at elevated temperatures.

The SnO_x species responsible for site blocking can be, at least to some extent, removed during subsequent CV scans, as demonstrated in Fig S5 of the Supplementary Material. After ten polarization cycles, regardless of the parent catalysts dispersion, the dissolution of SnO_2 formed upon exposition to air was almost stopped and, thus, the surface composition of the catalysts was stabilized. Considering the different dispersion of Pt and the presence of difficultly reducible SnO_2 in the (S-2) and (B-2) samples, it is not surprising that the highest electrochemically active Pt surface area ($ECSA_H$) data calculated from hydrogen desorption peaks were obtained for the Sn-Pt/C (S-0.5) sample.

As seen from the right panels of Fig. 4 a strong promotion of the CO oxidation process was observed on all Sn-modified samples when compared to the parent 20Pt/C catalysts. The onset potential ($E_{CO,onset}$) for the oxidation of CO on the Sn-20Pt/C catalysts was about 195-210 mV (see Table 2 and Fig. 4).

Promotional effect of SnO_2 in Sn-Pt/C electrocatalysts provided by the close proximity/contact of SnO_2 with Pt_3Sn alloy nanoparticles has been already demonstrated for the oxidation reaction of H_2, CO and H_2/CO mixtures [7,53] as well as for the oxygen reduction reaction (ORR) [9]. It is well-known [21] that these reactions are promoted by tin due to the formation of adsorbed OH_{ad} species at less positive potentials on Sn than on Pt.

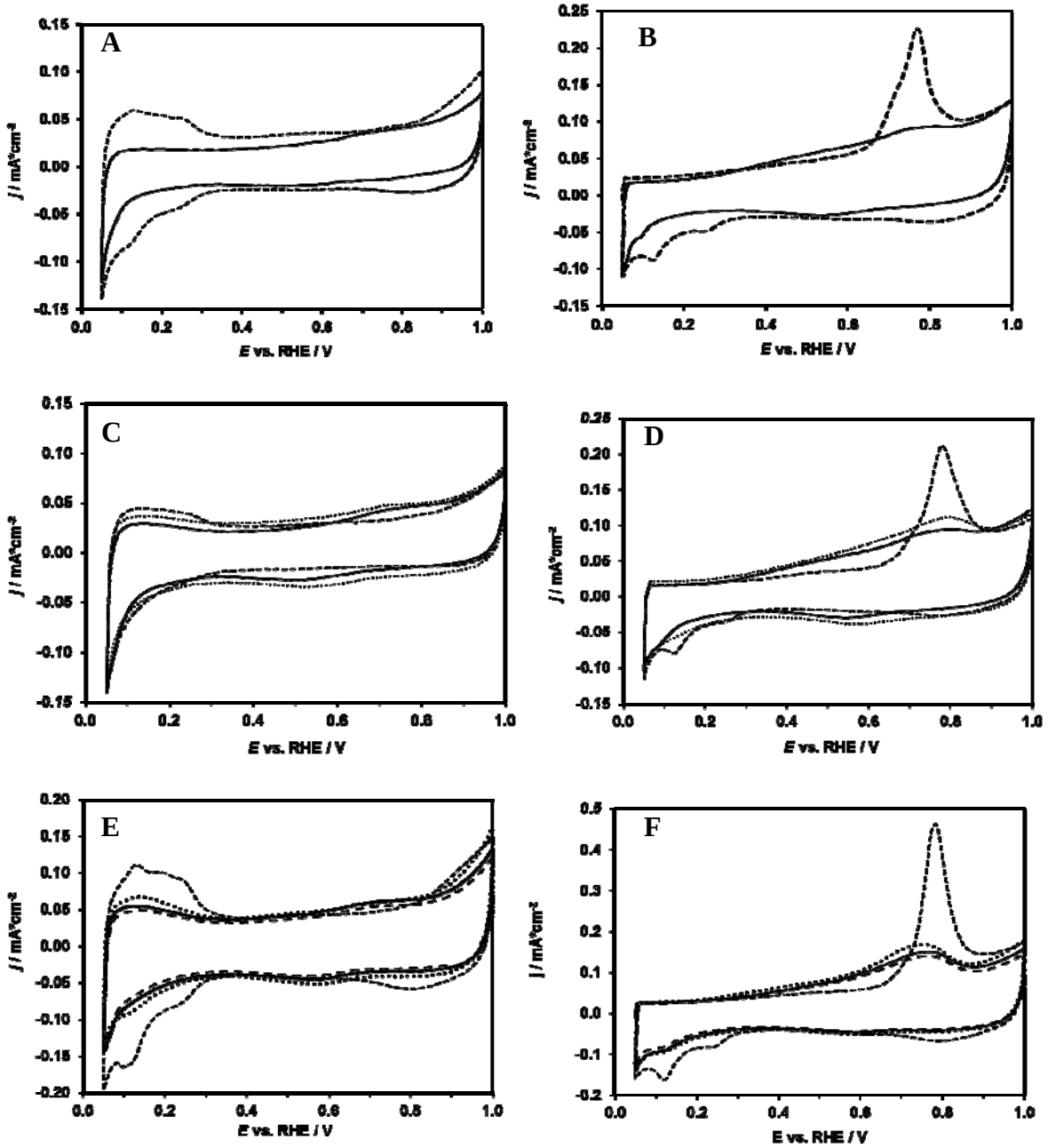

Fig. 4 The influence of tin introduction on the electrochemical behaviour. Cyclic voltammograms (left) and CO_{ads} stripping voltammograms (right) on the home-made 20Pt/C catalysts (short dashed line) and Sn-modified samples used without TPR (solid line). (A, B) the (S-2) type of samples; (C, D) the (B-2) type of samples; (E, F) the (S-0.5) type of samples; for comparison results obtained on the Sn-modified sample reduced at T_{red}= 250 °C (dashed line) and 350 °C (dotted line) are also included. Recorded in 0.5 M H_2SO_4 at 10 mV s^{-1}. The current was normalized to the geometric surface area.

$ECSA_{CO}$ values were also calculated from the CO-stripping measurements (see Table 2). As emerges from Table 2 after tin introduction onto the parent catalysts the decrease of the $ECSA_{CO}$ values were observed. It is necessary to mention that a challenge for the surface area determination is the appropriate choice of the integration limits and the subtraction of background currents [29]. As shown in Figs. 4B and S4B of the Supplementary Material the presence of increased amount of surface SnO_2 in Sn-modified catalysts with lower Pt

dispersion ((S-2) and (B-2)) results in an ill-defined shape of the CO-stripping curves with difficultly defined integration limits, therefore the corresponding $ECSA_{CO}$ values cannot be calculated precisely. A site-blocking effect caused by more pronounced SnO_2 segregation observed in these catalysts comparing to highly dispersed Sn-Pt/C (S-0.5) catalysts (see Scheme 1) results in a more significant decrease of the electrochemically active Pt surface area and, thus, in overall decrease of the activity in the CO electrooxidation.

The unique increase of the Pt-Sn(oxidized)/C catalyst ORR performance [9] was ascribed to a promoting effect of SnO_2 nano-islands segregated on the surface of Pt_3Sn core nanoparticles. In Ref. [9] a Pt-Sn(oxidized)/C catalyst was prepared by oxidation of the reduced carbon supported Pt-Sn alloy in a flow of 20 % O_2 in N_2 at 300 °C for 15 min. Based on the XPS results demonstrating the presence of difficulty reducible SnO_2 in our Sn-modified 20Pt/C catalysts with lower Pt dispersion ((S-2) and (B-2)) in close proximity/contact with Pt-Sn alloy phase, an increased catalytic activity and stability of these catalysts in ORR can be expected. Moreover the presence of the surface SnO_x in all our air exposed Sn-modified catalysts was also demonstrated by the XPS and electrochemical results. Thus, upon study of Sn-modified catalysts with different Pt dispersion the influence of the SnO_2 of various origins existing in close contact with Pt-Sn alloy phase on the performance in the ORR can be compared.

Catalytic activity of the catalyst samples was tested in the ORR by RDE technique in O_2 saturated 0.5 M H_2SO_4 solution at ambient temperature and pressure. Potential dynamic polarization curves (not shown) were obtained in oxygen saturated 0.5 M H_2SO_4 on RDE at different rotation speeds for all catalyst samples studied. Linear relationship was obtained between the square root of the rotation speed and the current density considering the current values corresponding to 300 mV potential. However, according to the Koutechky-Levic representation of the data the electrode reaction in all cases was under mixed kinetic-diffusion control at this potential.

In order to compare the catalysts mass specific current densities are depicted in Fig. 5. Oxygen reduction currents are normalized to the platinum content of the catalysts. Interpretation of the results of RDE measurements on electocatalysts with large surface area and disperse surface has to be carried out cautiously [54,55]. Nevertheless, in our case catalyst samples with similar composition and structure were investigated applying the same procedure and electrode preparation technique and the RDE results may contribute to the qualitative description and comparison the catalysts.

As shown in Fig. 4 and S5, upon modification with tin, electrochemically active Pt surface area of the catalysts decreased. At the same time, the Pt mass specific current densities of the ORR are significantly higher on all Sn-modified catalysts presented in Fig. 5 compared to the corresponding parent 20Pt/C catalysts (see curves 1 and 4 in Fig. 5) in the mixed kinetic-diffusion controlled region.

Marked difference has been found between the two groups of parent catalysts considering the onset potential of the ORR. As can be seen in Fig. 5 $\boldsymbol{j}$ vs. $\boldsymbol{E}$ curves of 20Pt/C (S-0.5) and the two Sn-modified version of this parent catalyst show very similar behaviour. Current densities on these samples in the kinetically controlled regime are significantly higher compared to the parent Pt/C (B-2) (curve 1 in Fig. 5) and Sn-modified (S-2) and (B-2) catalysts used without high-temperature reduction (see curves 2 and 3 in Fig. 5).

It is necessary to mention that reduction of the Sn-20Pt/C (B-2) catalyst at T_{red}= 250 °C results in significant increase in the mass specific current density (see curve 5 in Fig. 5); thus, the activity of this catalyst become comparable with the activity of the highly dispersed Sn-20Pt/C (S-0.5) sample used without TPR (see curve 6 in Fig. 5). It is important to note that in the case of the Sn-20Pt/C (S-0.5) catalyst the activity in the ORR was only slightly affected by the treatment applied after tin anchoring step I (compare curves 6 and 7 in

Fig. 5; the polarization curve obtained on the sample treated at T_{red}= 250 °C (not shown) was similar to the curve 7).

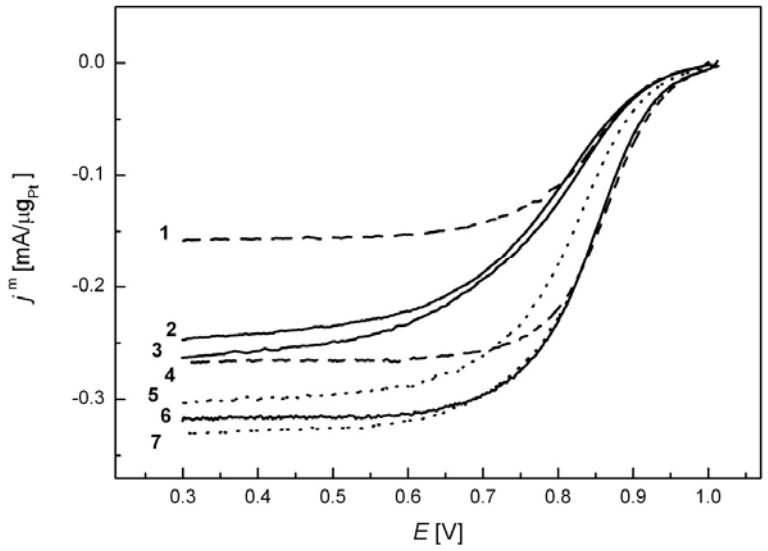

Fig. 5 Oxygen reduction mass specific current densities (negative sweep, 10 mV s^{-1}) measured in O_2 saturated 0.5 mol dm^3 H_2SO_4 on different Pt/C and Sn-Pt/C catalysts at 625 rpm. Parent catalysts (dashed line): 1: 20Pt/C (B-2), 4: 20Pt/C (S-0.5); Sn-modified catalysts used without TPR (solid line): 2: Sn-20Pt/C (S-2), 3: Sn-20Pt/C (B-2), 6: Sn-20Pt/C (S-0.5); Sn-modified catalysts used after TPR (dotted line): 5: Sn-20Pt/C (B-2), T_{red}= 250 °C; 7: Sn-20Pt/C (S-0.5), T_{red}= 350 °C.

As shown in Fig. 5 (compare curves 3 and 5) reduction of the Sn-20Pt/C (B-2) catalyst after tin anchoring step I at T_{red}= 250 °C results in pronounced current density increase. It can be proposed that the observed decrease of the bimetallic nanoparticles size (see Table 2), accompanied with decrease of the tin content on the platinum-support interface in this sample possibly leads to a Sn-Pt catalyst with optimal balance between SnO_2 nanoparticles and Pt_3Sn alloy phase.

In additional experiment the influence of the oxidative treatment used in Ref. [9] on the behavior of this catalyst in the ORR was also studied. After reduction at T_{red}= 250 °C the Sn-20Pt/C (B-2) sample was purged with nitrogen and then the catalyst was exposed to air at T_{oxid}= 250 °C for 15 min. We found that high-temperature oxidation of the Sn-Pt/C catalysts prepared by CSRs has negative influence on the ORR activity: the onset potential was shifted towards cathodic direction by 150 mV with respect to the parent Pt/C (B-2) (not shown); the current density value was the lowest comparing to other Sn-modified catalysts studied; moreover, the electrochemically active Pt surface area drastically decreased.

On the basis of the RDE measurements it can be concluded that highly dispersed Sn-20Pt/C (S-0.5) catalysts, which in accordance with the XPS results contain after reduction exclusively Pt-Sn alloy phases with Pt/Sn= 3, are the most promising in the ORR among the investigated samples.

Conclusions

In this contribution home-made 20Pt/C catalysts with different Pt dispersion were used for the preparation of alloy-type Sn-Pt/C electrocatalysts with desired Pt/Sn= 3.0 ratio by CSRs. Foremost, highly dispersed and stable Pt nanoparticles supported on active carbon

(Black Pearls 2000) were prepared by modified $NaBH_4$-assisted EG reduction method using ethanol as a solvent. Restricting the heating time of the ethanol solution containing the Pt precursor and carbon support before addition of the $NaBH_4$ and EG mixture to 0.5 h ((S-0.5) catalyst type) was found to increase the metal dispersion. On the contrary, increasing of the time of heating in ethanol up to 2 h results in a 20Pt/C catalysts with broad particle size distribution containing Pt particles ranging from small separated Pt clusters to Pt nanoparticles included in raspberry-like agglomerates ((S-2) and (B-2) catalysts type).

According to *in situ* XPS and *in situ* XRD studies upon using highly dispersed 20Pt/C (S-0.5) catalyst the exclusive incorporation of Sn onto the Pt sites was achieved resulting in exclusive formation of Pt-Sn alloy phase. No evidence of the presence of SnO_2 phase was found by means of the XRD and EDS analysis. In contrast to highly dispersed Sn-20Pt/C (S-0.5) catalyst, the reductive treatment of Sn-20Pt/C (S-2) catalyst with low Pt dispersion at 350°C does not result in complete reduction of the tin content. The major form of tin was attributed to the metallic Sn associated with Pt, while 10 % of tin was present in a form of Sn^{4+} surface species.

The electrocatalytic performance of the novel catalysts was tested in the CO oxidation and the ORR. Increased CO tolerance for all Sn-modified Pt/C catalysts compared to the parent 20Pt/C was demonstrated. The electrocatalytic performance of Sn-20Pt/C in the ORR is superior to that of the parent 20Pt/C catalysts. Small size of bimetallic nanoparticles and optimal surface composition of the Sn-20Pt/C (S-0.5) catalyst was responsible for an increased activity in the ORR. High-temperature reductive treatment applied after tin anchoring step II resulted in a subsequent increase of the ORR activity.

Acknowledgements
This work was supported by the National Development Agency [grant number KTIA_AIK_12-1-2012-0014]. Financial support by the Hungarian National Scientific Research Fund (OTKA) [grant numbers K100793 (Zoltán Pászti) and K112034 (István Bakos)] is greatly acknowledged.

References
[1] Martínez-Huerta MV, Rodríguez JL, Tsiouvaras N, Peña MA, Fierro JLG, Pastor E (2008) Novel Synthesis Method of CO-Tolerant PtRu-MoO_x Nanoparticles: Structural Characteristics and Performance for Methanol Electrooxidation. Chem Mater 20:4249-4259
[2] Guillén-Villafuerte O, García G, Rodríguez JL, Pastor E, Guil-López R, Nieto E, Fierro JLG (2013) Preliminary studies of the electrochemical performance of Pt/X@MoO_3/C (X = Mo_2C, MoO_2, Mo^0) catalysts for the anode of a DMFC: Influence of the Pt loading and Mo-phase. Int J Hydrogen Energy 38:7811-7821
[3] Martínez-Huerta MV, Rojas S, Gómez de la Fuente JL, Terreros P, Peña MA, Fierro JLG (2006) Effect of Ni addition over PtRu/C based electrocatalysts for fuel cell applications. Appl Catal B-Environ 69:75-84
[4] Liu CW, Chang YW, Wei YC, Wang KW (2011) The effect of oxygen containing species on the catalytic activity of ethanol oxidation for PtRuSn/C catalysts. Electrochim Acta 56:2574-2581
[5] Herranz T, Ibáñez M, Gómez de la Fuente JL, Pérez-Alonso FJ, Peña MA, Cabot A, Rojas S (2014) In Situ Study of Ethanol Electrooxidation on Monodispersed Pt_3Sn Nanoparticles. ChemElectroChem 1:12
[6] Antolini E, Gonzalez ER (2011) Effect of synthesis method and structural characteristics of Pt-Sn fuel cell catalysts on the electro-oxidation of CH_3OH and CH_3CH_2OH in acid medium. Catal Today 160:28-38

[7] Arenz M, Stamenkovic V, Blizanac BB, Mayrhofer KJ, Markovic NM, Ross PN (2005) Carbon-supported Pt-Sn electrocatalysts for the anodic oxidation of H_2, CO, and H_2/CO mixtures.: Part II: The structure–activity relationship. J Catal 232:402-410
[8] Takasaki F, Matsuie S, Takabatake Y, Noda Z, Hyashi S, Shirotori Y, Ito K, Sasaki K (2011) Carbon-Free Pt Electrocatalysts Supported on SnO_2 for Polymer Electrolyte Fuel Cells: Electrocatalytic Activity and Durability. J Electrochem Soc 158:B1270-B1275
[9] Samjeské G, Nagamatsu S, Takao S, Nagasawa K, Imaizumi Y, Sekizawa O, Yamamoto T, Uemura Y, Uruga T, Iwasawa Y (2013) Performance and characterization of a Pt-Sn(oxidized)/C cathode catalyst with a SnO_2-decorated Pt_3Sn nanostructure for oxygen reduction reaction in a polymer electrolyte fuel cell. Phys Chem Chem Phys 15:17208-17218
[10] Margitfalvi JL, Borbáth I, Tfirst E, Tompos A (1998) Formation of multilayered tin organometallic surface species. Preparation of new type of supported Sn-Pt catalysts. (1998) Catal Today 43:29-49
[11] Margitfalvi JL, Borbáth I, Hegedűs M, Tfirst E, Gőbölös S, Lázár K (2000) Low-Temperature CO Oxidation over New Types of Sn-Pt/SiO_2 Catalysts. J Catal 196:200-204
[12] Margitfalvi JL, Borbáth I, Hegedűs M, Tompos A (2002) Preparation of new type of Sn-Pt/SiO_2 catalysts for carbonyl activation. Appl Catal A-Gen 229:35-49
[13] Borbáth, I. (2013) *Preparation of bi- and multimetallic supported catalysts by controlled surface reactions*. PhD Dissertation, Budapest University of Technology and Economics, Budapest, Hungary, pp. 124. Retrieved from http://hdl.handle.net/10890/1297
[14] Borbáth I, Somodi F, Vilella IMJ, de Miguel SR, Scelza OA, Margitfalvi JL (2009) Differences and similarities of supported Ge-Pt/C catalysts prepared by conventional impregnation and controlled surface reactions. Catal Commun 10:490-493
[15] Margitfalvi JL, Borbáth I, Lázár K, Tfirst E, Szegedi Á, Hegedűs M, Gőbölös S (2001) In Situ Characterization of Sn-Pt/SiO_2 Catalysts Used in Low Temperature Oxidation of CO. J Catal 203:94-103
[16] Margitfalvi JL, Gőbölös S, Tálas E, Borbáth I In: Eguchi K, Machida M, Yamanaka I (Eds.) (2006) Science and Technology in Catalysis (STUDIES IN SURFACE SCIENCE AND CATALYSIS, 172) Amsterdam-Tokyo, Elsevier-Kodansha, 2007, *pp. 177-180*
[17] Margitfalvi JL, Vankó Gy, Borbáth I, Tompos A, Vértes A (2000) Characterization of Sn-Pt/SiO_2 Catalysts Used in Selective Hydrogenation of Crotonaldehyde by Mössbauer Spectroscopy. J Catal 190:474-477
[18] Vilella IM, Borbáth I, Margitfalvi JL, Lázár K, de Miguel SR, Scelza OA (2007) PtSn/SiO_2 catalysts prepared by controlled surface reactions for citral hydrogenation in liquid phase. Appl Catal A-Gen 326:37-47
[19] Bocanegra SA, de Miguel SR, Borbath I, Margitfalvi JL, Scelza OA (2009) Behavior of bimetallic PtSn/Al_2O_3 catalysts prepared by controlled surface reactions in the selective dehydrogenation of butane. J Mol Catal A-Chem 301:52-60
[20] García-Rodríguez S, Somodi F, Borbáth I, Margitfalvi JL, Peña MA, Fierro JLG, Rojas S (2009) Controlled synthesis of Pt-Sn/C fuel cell catalysts with exclusive Sn-Pt interaction: Application in CO and ethanol electrooxidation reactions. Appl Catal B-Environ 91:83-91
[21] Borbáth I, Gubán D, Pászti Z, Sajó IE, Drotár E, Gómez de la Fuente JL, Herranz T, Rojas S, Tompos A (2013) Controlled Synthesis of Pt_3Sn/C Electrocatalysts with Exclusive Sn-Pt Interaction Designed for Use in Direct Methanol Fuel Cells. Top Catal 56:1033-1046
[22] Herranz T, García S, Martínez-Huerta MV, Peña MA, Fierro JLG, Somodi F, Borbáth I, Majrik K, Tompos A, Rojas S (2012) Electrooxidation of CO and methanol on well-characterized carbon supported Pt_xSn electrodes. Effect of crystal structure. Int J Hydrogen Energy 37:7109-7118
[23] Hwang IC, Ji JH, Kim P, Joo JB US Patent 7,838,458 B2 United States of America 23 Nov 2010

[24] Fairley N (2006) www.casaxps.com
[25] Mohai M (2004) MultiQuant: multimodel XPS quantification software. Surf Interface Anal 36:828-832
[26] Mohai M (2003) XPS MultiQuant: Multi-model X-ray photoelectron spectroscopy quantification program, Version 3.00.16 http://www.chemres.hu/aki/XMQpages/XMQhome.htm
[27] Wagner CD, Naumkin AV, Kraut-Vass A, Allison JW, Powell CJ, Rumble Jr JR (2003) NIST X-ray Photoelectron Spectroscopy Database, Version 3.4, National Institute of Standards and Technology, Gaithersburg, MD, (http://srdata.nist.gov/xps/)
[28] Moulder JF, Stickle WF, Sobol PE, Bomben KD (1992) Handbook of X-ray Photoelectron Spectroscopy, Perkin-Elmer Corp., Eden Prairie, Minnesota, USA
[29] Schulenburg H, Durst J, Müller E, Wokaun A, Scherer GG (2010) Real surface area measurements of Pt_3Co/C catalysts. J Electroanal Chem 642:52-60
[30] Yan Z, Wang M, Lu Y, Liu R, Zhao J (2014) Ethylene glycol stabilized $NaBH_4$ reduction for preparation carbon-supported Pt-Co alloy nanoparticles used as oxygen reduction electrocatalysts for microbial fuel cells. J Solid State Electrochem 18:1087-1097.
[31] Kim P, Joo JB, Kim W, Kim J, Song IK, Yi J (2006) $NaBH_4$-assisted ethylene glycol reduction for preparation of carbon-supported Pt catalyst for methanol electro-oxidation. J Power Sources 160(2): 987-990.
[32] Joo JB, Kim P, Kim W, Kim Y, Yi J (2009) Effect of the preparation conditions of carbon-supported Pt catalyst on PEMFC performance. J Appl Electrochem 39: 135-140.
[33] Duff DG, Mallat T, Schneider M, Baiker A (1995) Catalysts derived from polymer-stabilised colloidal platinum: Effects of support and calcination on the catalytic behaviour in hydrogenation. Appl Catal A-Gen 133:133-148
[34] Choo HP, Liew KY, Liu HF, Seng CE (2001) Hydrogenation of palm olein catalyzed by polymer stabilized Pt colloids. J Mol Catal A-Chem 165:127-134
[35] Choo HP, Liew KY, Liu HF, Seng CE, Mahmood WAK, Bettahar M (2003) Activity and selectivity of noble metal colloids for the hydrogenation of polyunsaturated soybean oil. J Mol Catal A-Chem 191:113-121
[36] Chen CW, Serizawa T, Akashi M (1999) Preparation of Platinum Colloids on Polystyrene Nanospheres and Their Catalytic Properties in Hydrogenation. Chem Mater 11:1381-1389
[37] Xu Q, Liu XM, Chen JR, Li RX, Li XJ (2006) Hydrogenation of aromatics over supported noble metal catalysts ex organometallic complexes. J. Mol. Catal. A-Chem 260:299-305
[38] Maillard F, Schreier S, Hanzlik M, Savinova ER, Weinkauf S, Stimming U (2005) Influence of particle agglomeration on the catalytic activity of carbon-supported Pt nanoparticles in CO monolayer oxidation. Phys. Chem. Chem. Phys. 7: 385-393.
[39] Maillard F, Peyrelade E, Soldo-Olivier Y, Chatenet M, Chaînet E, Faure R (2007) Is carbon-supported Pt-WO_x composite a CO-tolerant material? Electrochim Acta 52:1958-1967
[40] Margitfalvi JL, Borbáth I, Hegedűs M, Gőbölös S (2001) Modification of alumina supported platinum catalyst by tin tetraethyl in a circulation reactor. Appl Catal A-Gen 219:171-182
[41] Torres GC, Jablonski EL, Baronetti GT, Castro AA, de Miguel SR, Scelza OA, Blanco MD, Pena Jiménez MA, Fierro JLG (1997) Effect of the carbon pre-treatment on the properties and performance for nitrobenzene hydrogenation of Pt/C catalysts. Appl Catal A-Gen 161:213-226
[42] de Miguel SR, Roman-Martinez MC, Jablonski EL, Fierro JLG, Cazorla-Amoros D, Scelza OA (1999) Characterization of Bimetallic PtSn Catalysts Supported on Purified and H2O2-Functionalized Carbons Used for Hydrogenation Reactions. J Catal 184:514-525

[43] Román-Martinez MC, Cazorla-Amorós D, Linares-Solano A, Salinas-Martinez de Lecea C, Yamashita H, Anpo M (1995) Metal-support interaction in Pt/C catalysts. Influence of the support surface chemistry and the metal precursor. Carbon 33:3-13
[44] Harris IR, Norman M, Brayant AW (1968) A study of some palladium-indium, platinum-indium and platinum-tin alloys. J Less-Common Met 16: 427-440
[45] Cs. Vèrtes Cs, E. Tálas E, I. Czakó-Nagy I, J. Ryczkovski J, S. Gőbölös S, A. Vèrtes A, J. Margitfalvi J (1991) Mössbauer spectroscopy studies of Sn-Pt/Al_2O_3 catalysts prepared by controlled surface reactions Appl Catal 68: 149-159
[46] Moscu A, Veyre L, Thieuleux C, Meunier F, Schuurman Y (2015) CO PROX over Pt-Sn/Al_2O_3: A combined kinetic and in situ DRIFTS study. Catal Today 258:241-246
[47] Jerdev DI, Koel BE (2001) Oxidation of ordered Pt-Sn surface alloys by O_2. Surf Sci 492:106-114
[48] Axnanda S, Zhou WP, White MG (2012) CO oxidation on nanostructured SnO_x/Pt(111) surfaces: Unique properties of reduced SnO_x. Phys Chem Chem Phys 14:10207-10214
[49] Michalak WD, Krier JM, Alayoglu S, Shin J, An K, Komvopoulos K, Liu Z, Somorjai GA (2014) CO oxidation on PtSn nanoparticle catalysts occurs at the interface of Pt and Sn oxide domains formed under reaction conditions. J Catal 312:17-25
[50] Virnovskaia A, Jorgensen S, Hafizovic J, Prytz O, Kleimenov E, Havecker M, Bluhm H, Knop-Gericke A, Schlögl R, Olsbye U (2007) In situ XPS investigation of Pt(Sn)/Mg(Al)O catalysts during ethane dehydrogenation experiments. Surf Sci 601:30-43
[51] Bouwman R, Biloen P (1974) Surface analysis of platinum/tin alloys by x-ray photoelectron spectroscopy. Anal Chem 46:136-138
[52] Merlen E, Beccat P, Bertolini JC, Delichere P, Zanier N, Didillon B (1996) Characterization of Bimetallic Pt-Sn/Al_2O_3 Catalysts: Relationship between Particle Size and Structure. J Catal 159:178-188
[53] Radmilovic V, Richardson TJ, Chen SJ, Ross Jr PN (2005) Carbon-supported Pt-Sn electrocatalysts for the anodic oxidation of H_2, CO, and H_2/CO mixtures. Part I. Microstructural characterization. J Catal 232:199-209
[54] Masa J, Batchelor-McAuley C, Schuhmann W, Compton RG (2014) Koutecky-Levich analysis applied to nanoparticle modified rotating disk electrodes: Electrocatalysis or misinterpretation. Nano Res 7:71-78
[55] Batchelor-McAuley C, Compton RG (2014) Thin-film modified rotating disk electrodes: Models of electron-transfer kinetics for passive and electroactive films. J Phys Chem C 118:30034-30038

Supplementary material for

CO oxidation and oxygen reduction activity of bimetallic Sn-Pt electrocatalysts on carbon: effect of the microstructure and the exclusive formation of the Pt_3Sn alloy

D. Gubán[1], A. Tompos[1], I. Bakos[1], Z. Pászti[1], G. Gajdos[1], I. Sajó[2], I. Borbáth[1*]

[1] *Institute of Materials and Environmental Chemistry, Research Centre for Natural Sciences, Hungarian Academy of Sciences, H-1117 Budapest, Magyar tudósok körútja 2, Hungary*
[2] *University of Pécs, Szentágothai Research Centre, Pécs, H-7624, Ifjúság str. 20, Hungary*

1. Details of the modification of the Pt/C catalysts by tin

200 mg of the Pt/C catalyst was suspended in 10 ml *n*-decane. The autoclave was purged for 10 minutes by means of hydrogen and then the hydrogen pressure was set up to 5 bars. The reactor was immersed in an oil bath and heated up to 170°C, then the tin anchoring reaction was started by consecutive addition of the appropriate amount of 0.03 M $Sn(C_2H_5)_4$ solution in decane. For this purpose the calculated amount of tetraethyltin (needed for the preparation of Sn-Pt/C catalysts with desired Pt/Sn=3.0 ratio) was divided into five equal portions (456 µl) and introduced under vigorous stirring into the reactor after equal periods of time (45 minutes). After that the next portion of decane solution of tetraethyltin was added. After the modification procedure, the catalyst was separated by centrifugation and carefully washed twice with 20 ml *n*-decane and tree times with 20 ml *n*-hexane. The catalyst was dried in air at 60°C overnight.

Before and after the modification procedure the concentration of the solutions of the $Sn(C_2H_5)_4$ in decane was analyzed by Nicolet Avatar 320 FT-IR spectrometer [S1]. The ν_{Sn-C} stretching band at 507 cm^{-1} (spectrum not shown) was used for the measuring the completion of the surface reaction between the Pt and the tetraethyltin.

After the surface modification the catalysts have been treated in hydrogen atmosphere by Temperature Programmed Reduction (TPR) technique using the following experimental parameters: heating rate= 5°C min^{-1}, hydrogen flow rate= 30 ml min^{-1}. The final temperature (T_{red}) applied during TPR (reaction (2)) was 250 or 350°C. Catalysts were kept at final temperature for 2 hours then the furnace was cooled down in flowing hydrogen to 50°C. The atmosphere was changed to nitrogen and the system was cooled down to room temperature under flowing nitrogen atmosphere.

Blank experiment performed at T_r= 170°C and P_{H2}= 5 bar with pure carbon support and 0.03 M $SnEt_4$ solution in *n*-decane showed that no reaction proceed. The tin content was analyzed by ICP-OES.

2. Details of the physicochemical characterization

2.1. X-ray Diffraction

In situ X-Ray Diffraction (XRD) experiments were carried out by a Philips model PW 3710 based PW 1050 Bragg-Brentano parafocusing goniometer in a heatable sample holder Anton Paar HTK 1200 using CuK_α radiation (λ= 0.15418 nm) operating at 40 kV and 35 mA, graphite monochromator and proportional counter. Silicon powder (NIST SRM 640) was used as an internal standard and the scans were evaluated with profile fitting methods. The cell parameters of the crystalline phases were determined from the fitted d-values. Crystallite sizes were calculated from reflection line broadening using the Scherrer-equation.

* Corresponding author, Tel.: +36 1 382 6916, email: borbath.irina@ttk.mta.hu, address: H-1519 Budapest, P.O.Box 286, Hungary (Irina Borbáth)

About 50 mg catalyst sample was loaded into the cell and a powder XRD measurement was carried out in the 2 theta range of 10 to 90 degrees at a scanning speed of 0.02° s^{-1}. Then after purging with N_2 for 15 min the sample was heated up to 200°C with a rate of 5°C min^{-1} in H_2 flow and kept at constant temperature for 2 h, then another XRD pattern was recorded as described earlier. The same procedure was repeated at 250, 300 and 350°C, respectively. After the measurements the sample was cooled down to RT in H_2 and XRD pattern was recorded. Then after purging with N_2 15 min the sample was exposed to air for 24 h and then XRD measurements were carried out again.

2.2 Energy dispersice X-ray spectrometry (EDS)

Energy Dispersive X-ray Spectrometry (EDS) analysis was performed with an INCA (Oxford Instruments Ltd.) detector and the INCAEnergy software package. EDS analysis of individual particles was possible by using ZEISS EVO 40XVP Scanning Electron Microscope (accelerating voltage: 20kV, W-filament).

2.3 X-ray Photoelectron Spectroscopy (XPS)

X-ray photoelectron spectroscopy (XPS) measurements were carried out using an EA 125 electron spectrometer manufactured by OMICRON Nanotechnology GmbH (Germany) operated in the Constant Analyser Energy mode with 30 eV pass energy resulting in a spectral resolution of 1 eV. The photoelectrons were excited by MgKα (1253.6 eV) radiation.

Samples in the form of fine powder were suspended in hexane. Drops of this suspension were placed on standard OMICRON sample plates; after evaporation of hexane catalyst coatings with sufficient adhesion and electric conductivity were obtained. The sample was first analyzed in the "as received" state. The next measurement was made after reduction in the high pressure cell of the spectrometer in 300 mbar H_2 at different temperatures for 2 hours.

3. Cyclic voltammetry and CO_{ad} stripping voltammetry of the 20Pt/C (S-0.5), the 20Pt/C (S-2) and the 20Pt/C (B-2) parent electrocatalysts

The electrochemical behavior of the 20Pt/C electrocatalysts prior to modification by Sn was studied by cyclic voltammetry and CO_{ad} stripping. The obtained voltammograms are presented in Fig. S1.

All home-made 20Pt/C electrocatalysts have characteristic hydrogen adsorption/desorption features in the range between $0.05 < E < 0.4$ V and enlarged double layer region (see Fig. S1A). Increased double layer can be related to the big surface area (1475 m^2 g^{-1}) and increased number of the surface functional groups of the Black Pearls 2000 carbon support.

As can be seen from Fig. S1B and Table 1 of the main text the onset potential ($E_{CO,onset}$) for the oxidation of CO on the home-made Pt/C catalysts was about 615-625 mV with the main CO_{ad} stripping peak maximum ($E_{CO,max}$) at about 765-785 mV.

According to literature data not only the size but even the nanostructure of the platinum (the agglomeration of Pt nanoparticles and formation of nano-grained structures with high surface defect density) influences strongly the peak maximum observed upon CO oxidation [S2]. Different peak positions are reported for Pt agglomerates and isolated Pt nanoparticles [S2], which alone leads to some dependence of the apparent peak position on the particle size. It has been shown that CO stripping voltammetry provides a fingerprint of the particle size distribution and the extent of particle agglomeration in carbon-supported Pt catalysts [S3]. The presence of two electrooxidation peaks at 760 and 840 mV in Pt-based catalysts was ascribed by Maillard *et al.* [S2] to the CO oxidation on Pt nanoparticles with different size and structures (the peaks at 840 mV and 760 mV were related to small isolated

single crystalline Pt nanoparticles and Pt agglomerates, respectively [S3]). Enhanced catalytic activity of Pt agglomerates composed of interconnected nm-sized metal grains was ascribed to high concentration of surface defects in Ref. [S3].

Similar tendency was observed in the present study. Electrochemical CO monolayer oxidation is influenced by the size of Pt nanoparticles, the smaller the particle size, the higher the reaction overpotential (see Table 1 of the main text).

In addition, the morphological differences between the 20Pt/C catalysts are reflected by the shape of the CO oxidation peak. As shown in Fig. S1B the increased Pt particle size of the 20Pt/C (S-2) or (B-2) catalyst compared to the (S-0.5) sample results in a considerable decrease of the main CO oxidation peak and, as a consequence, in decrease of the electrochemically active Pt surface area of the main text (see $ECSA_{CO}$ values in Table 1 of the main text). Also, on the CO_{ad} stripping curves of both catalyst samples containing raspberry-like agglomerates ((S-2) and (B-2)) a shoulder at lower overpotential (ca. 705-715 mV) was observed (see Fig. S1B); this feature may be related to the presence of highly disordered surface defects in the interconnected particles.

A detailed discussion of the possible origin of the main peak shift in CO_{ads} electrooxidation at Pt nanoparticles surface is beyond the scope of this paper but is available in the above mentioned references [S2,S3].

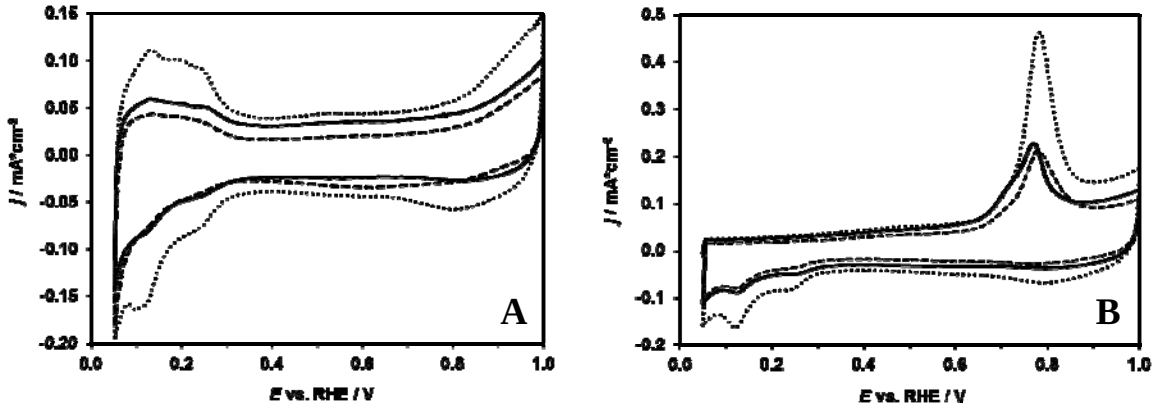

Fig. S1. Cyclic voltammograms (A) and CO_{ads} stripping voltammograms (B) of the home-made 20Pt/C catalysts: 20Pt/C (S-2) (solid line), 20Pt/C (B-2) (dashed line) and 20Pt/C (S-0.5) (dotted line). Recorded in 0.5 M H_2SO_4 at 10 mV s^{-1}. The current was normalized to the geometric surface area.

According to the above results, the electrochemical measurements performed on the unmodified parent catalysts reflect well the morphological differences. Not surprisingly, the best electrochemical performance in CO_{ad} stripping was observed on the highly dispersed 20Pt/C (S-0.5) catalyst.

4. Scanning electron microscopy and Energy dispersive X-ray spectrometry analysis

SEM and EDS analysis (Fig. S2) of different regions of the Sn-20Pt/C (S-2) catalyst sample reveals the coexistence of Sn and Pt particles with Pt/Sn atomic ratio of 3, which agrees well with the nominal Pt/Sn atomic ratio. No evidence of Sn segregation was evidenced. Based on the EDS results an average content of the Sn-20Pt/C (S-2) sample was 22.6 ± 1.4 wt.% of Pt and 3.8 ± 0.6 wt.% of Sn, which agrees closely with expected values (Pt= 20 wt.% and Sn= 4 wt.%).

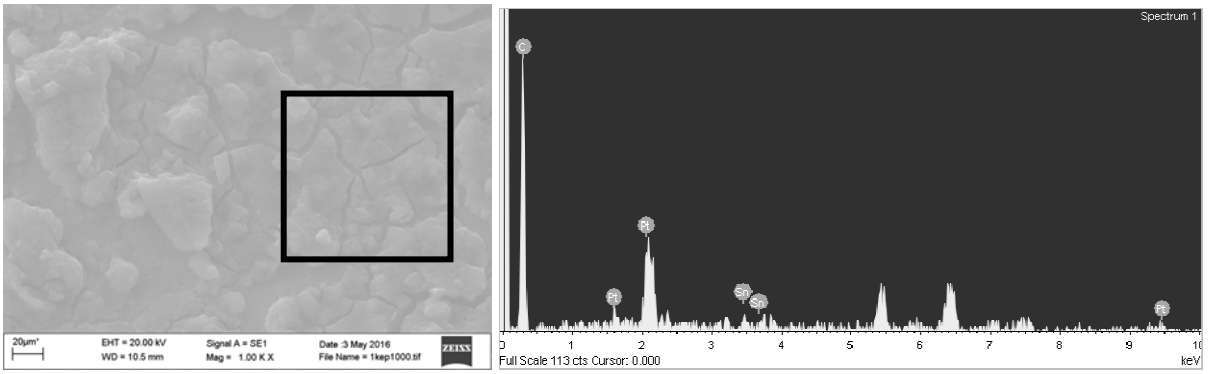

Fig. S2. SEM image and EDS spectrum of the Sn-Pt/C (S-2) catalyst. The black rectangle in the SEM image shows the selected EDS inspection field.

5. XRD studies of the Sn-20Pt/C (S-0.5) electrocatalyst

It is well known that upon increasing tin content the lattice parameter changes linearly from 3.9231 Å for pure Pt (PDF#04-0802) to 4.0015 Å for Pt_3Sn alloy (PDF#35-1360). Thus the incorporation of tin into the fcc structure of platinum results in shift of the peaks to lower 2θ values.

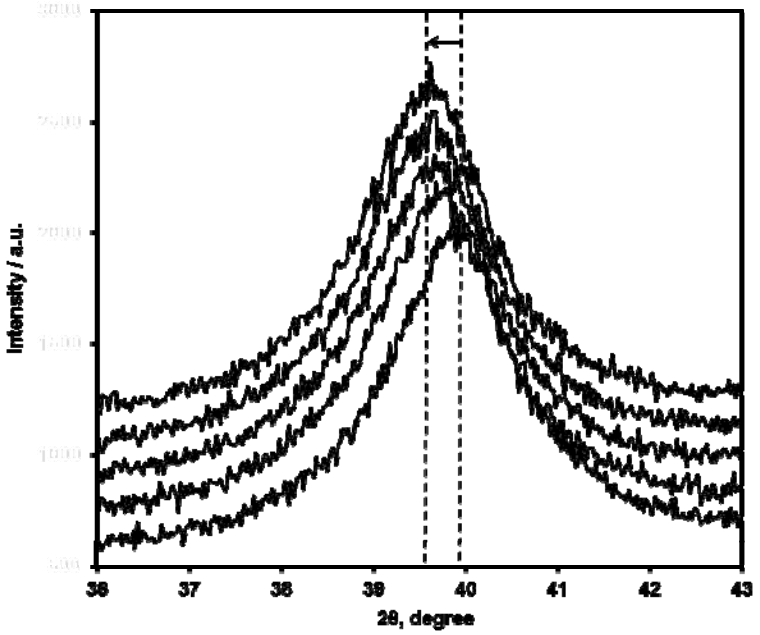

Fig. S3. X-ray diffraction pattern of the Sn-20Pt/C (S-0.5) catalyst. Influence of the treatment *in situ* in H_2 atmosphere at different temperatures on the position of the most intense reflection is shown (for details see Table 3 and Experimental part). The arrow indicates the direction of changes observed upon increase of the reduction temperature from 25°C up to 350°C.

The Sn-20Pt/C (S-0.5) catalyst sample used after tin anchoring step I without any high-temperature treatment was studied by *in situ* XRD technique (for details see the Experimental part). Fig. S3 shows the influence of different reduction temperatures on the position of the Pt(111) reflection. The XRD pattern of the air stored Sn-20Pt/C (S-0.5) catalyst used without TPR can be fitted to the pure fcc Pt crystalline phase. As evidenced from the XRD patterns depicted in Fig. S3, upon increasing the temperature of the reduction the peak shifted to lower 2θ values. After *in situ* treatment in H_2 at 350°C for 2 h (see line 2 in

Table 3) the refined lattice constant of the Pt-Sn alloy was a= 3.955 Å (between those of Pt_3Sn and $Pt_{90}Sn_{10}$) with average crystallite size of 6.6 nm. The lattice constant value calculated for catalyst reduced *in situ* was higher than that one obtained after *ex situ* reduction (see lines 1 and 2 in Table 3), demonstrating that *in situ* XRD treatment results in the Pt-Sn alloy phase with higher Sn content in the Pt lattice (10 at.% < Sn < 25 at.%), confirming that a certain fraction of tin still remained in a non-alloyed, X-ray amorphous form under the *ex situ* reduction at 350°C.

6. Cyclic voltammetry and CO_{ad} *stripping voltammetry of the Sn-20Pt/C electrocatalysts used without TPR*

Fig. S4 compares the CVs and CO-stripping curves recorded on three Sn-modified catalysts used after modification and drying procedure, without high-temperature reduction. The CVs of the tin-modified samples showed the rather suppressed hydrogen adsorption/desorption region. A site-blocking effect caused by tin segregation can be a reason of the pronounced decrease of H_2 adsorption/desorption. As can be seen from Fig. S4A a site-blocking effect is more pronounced in a case of catalysts containing raspberry-like Pt agglomerates ((S-2) and (B-2)).

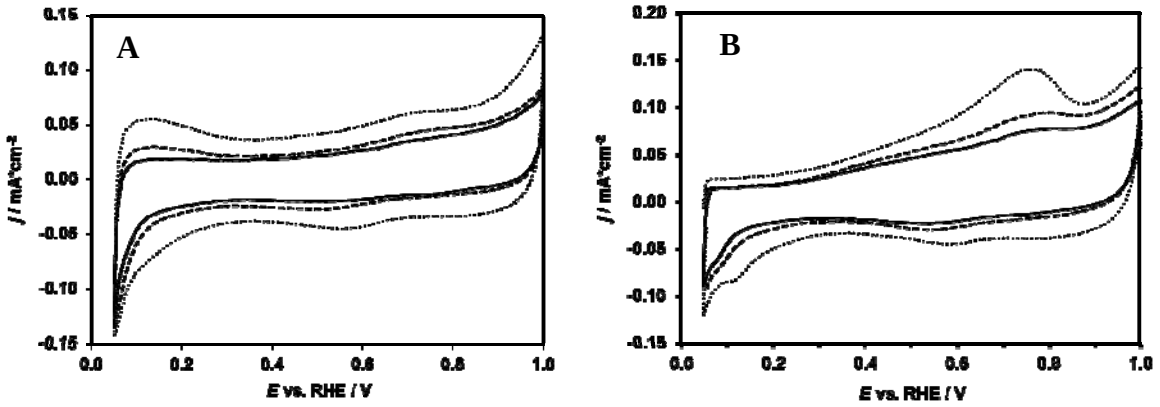

Fig. S4 Cyclic voltammograms (A) and CO_{ads} stripping voltammograms (B) of the Sn-modified home-made Sn-20Pt/C catalysts used without TPR: Sn-20Pt/C (S-2) (solid line), Sn-20Pt/C (B-2) (dashed line) and Sn-20Pt/C (S-0.5) (dotted line). Recorded in 0.5 M H_2SO_4 at 10 mV s^{-1}. The current was normalized to the geometric surface area.

As shown in Fig. S4B the presence of increased amount of surface SnO_2 in Sn-modified catalysts with lower Pt dispersion ((S-2) and (B-2)) results in an ill-defined shape of the CO-stripping curves. A site-blocking effect caused by more pronounced SnO_2 segregation observed in these catalysts comparing to highly dispersed Sn-Pt/C (S-0.5) catalysts (see Scheme 1 of the main text) results in a more significant decrease of the electrochemically active Pt surface area and, thus, in overall decrease of the activity in the CO electrooxidation.

7. Change of $ECSA_H$ *data during subsequent CV cycles*

In a series of experiments the influence of the number of the polarization cycles on the surface composition change of parent 20Pt/C catalysts and corresponding Sn-modified samples was demonstrated (see Fig. S5). Electrochemically active Pt surface area ($ECSA_H$) data were calculated from hydrogen desorption peaks of the cyclic voltammograms.

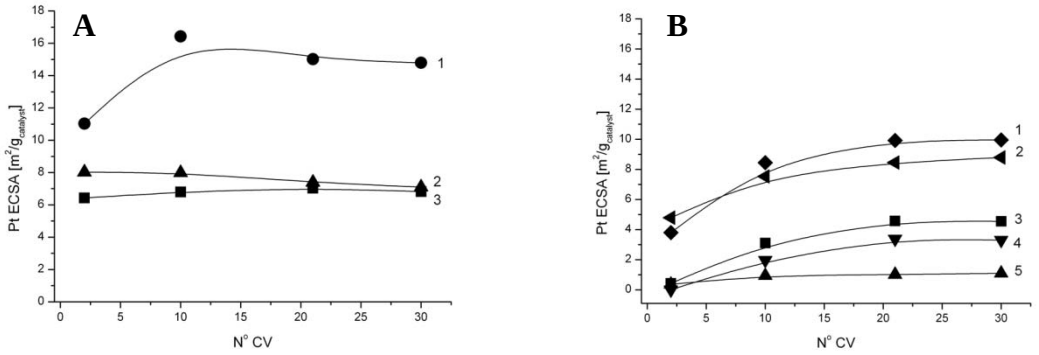

Fig. S5. Surface composition change of catalyst samples during cyclic polarization. Electrochemically active Pt surface area obtained from hydrogen desorption peaks of the cyclic voltammograms as a function of the number of cycles. **(A)** Parent 20Pt/C catalysts: Curve 1: 20Pt/C (S-0.5); 2: 20Pt/C (S-2); 3: 20Pt/C (B-2); and **(B)** Sn-modified catalysts: Curve 1: Sn-20Pt/C (S-0.5), T_{red}= 350 °C; 2: Sn-20Pt/C (S-0.5), without TPR; 3: Sn-20Pt/C (B-2), T_{red}= 250 °C; 4: Sn-20Pt/C (B-2), without TPR; 5: Sn-20Pt/C (S-2), without TPR. Lines serve as guides to the eye.

As shown in Fig. S5, the dilution of the Pt with Sn, which appears during modification by CSRs, resulted in decrease of the electrochemically active Pt surface area. The highest $ECSA_H$ value was calculated for 20Pt/C (S-0.5) catalyst (see curve 1 in Fig. S5A). Some increase of the $ECSA_H$ value, observed on this catalyst between 2nd and 10th cycles, can be related to the cleaning of the electrode surface from the residual impurities. The $ECSA_H$ values calculated for the parent and tin-modified catalysts with lower dispersion ((S-2) and (B-2) catalysts) were twice smaller than the corresponding values calculated for the 20Pt/C (S-0.5) (Fig. S5A) and Sn-20Pt/C (S-0.5) catalysts (Fig. S5B). After pre-treatment of the Sn-modified samples in H_2 the $ECSA_H$ values were only slightly higher compared to those one obtained of the Sn-20Pt/C samples used after tin anchoring step I without TPR (compare curves 1 and 2 with curves 3 and 4 in Fig. S5). The behavior of all tin-modified Pt/C catalysts is quite similar: an increase of the $ECSA_H$ values between 2nd and 10th cycles and relative stability of the surface composition after 20th cycle. However, it is important to note that after ten polarization cycles, regardless of the parent catalysts dispersion, the dissolution of SnO_2 formed upon exposition to air was almost stopped and, thus, the surface composition of the catalysts was stabilized.

References

[S1] Herranz T, García S, Martínez-Huerta MV, Peña MA, Fierro JLG, Somodi F, Borbáth I, Majrik K, Tompos A, Rojas S (2012) Electrooxidation of CO and methanol on well-characterized carbon supported Pt_xSn electrodes. Effect of crystal structure. Int J Hydrogen Energy 37:7109-7118

[S2] Maillard F, Peyrelade E, Soldo-Olivier Y, Chatenet M, Chaînet E, Faure R (2007) Is carbon-supported Pt-WO_x composite a CO-tolerant material? Electrochim Acta 52:1958-1967.

[S3] Maillard F, Schreier S, Hanzlik M, Savinova ER, Weinkauf S, Stimming U (2005) Influence of particle agglomeration on the catalytic activity of carbon-supported Pt nanoparticles in CO monolayer oxidation. Phys. Chem. Chem. Phys. 7: 385-393.